Montanuniversitaet Leoben

Master Thesis

Department of Applied Geophysics

Petrographic Coded Modelling of Thermal Conductivity

Markus KIENLER (0935284)

Supervisor: Dipl.-Ing. Dr.mont. Nina GEGENHUBER

July 2015

Affirmation

I declare in lieu of oath, that I wrote this thesis and performed the associated research myself, using only literature cited in this volume.

Leoben, July 2015

Markus Alfred Kienler

Acknowledgement

I am using this opportunity to express my gratitude to everyone who supported me throughout my Master thesis.

First of all, I am very thankful to my supervisor, Dipl.-Ing. Dr.mont. Nina Gegenhuber for her aspiring guidance and constructive criticism. She always found time to answer my questions and gave me new points of view for my Master thesis.

I express my warm thanks to Hon.Prof.Dr.rer.nat.habil. Jürgen Schön for his support and for explaining things in a very understanding way.

I would also like to thank the Chair of Applied Geophysics at the Montanuniversitaet Leoben for providing me with all the laboratory data. A big thank you also goes to Christiane Pretzenbacher for all her work, support and assistance.

My family has been encouraging, supportive and shown belief in me and my work. They have always been a strong backing in hard times.

Last but not least I want to thank my girlfriend Simone for all her love and pushing me all the time.

Thank you!

Markus Kienler

Zusammenfassung

Im Zuge dieser Diplomarbeit wird auf den Zusammenhang der Wärmeleitfähigkeit mit verschiedenen petrophysikalischen Parametern (elektrischer Widerstand, Kompressionswellengeschwindigkeit) eingegangen. Als Grundlage für die verschiedenen Modellberechnungen dienen Labormessungen des Lehrstuhles für Angewandte Geophysik an der Montanuniversität Leoben. Bei den meisten Bohrlochprojekten sind Kerndaten oftmals nicht vorhanden und eine indirekte Ermittlung der Wärmeleitfähigkeit der verschiedenen Gesteinsschichten würde zu einer großen Kostenersparnis führen.

Zu diesem Zweck werden die Labordaten nach verschiedenen Lithologien getrennt. Danach erfolgt eine Unterteilung der Proben anhand des Porenraumes mithilfe von elektrischen Eigenschaften. Im nächsten Schritt wird die Wärmeleitfähigkeit der Gesteinsmatrix unter Berücksichtigung von Zementationsfaktor und Porenform (aspect ratio) ermittelt. Mit Modelrechnungen (Inklusion-Model) ist es nun möglich den Zusammenhang von elektrischen Eigenschaften bzw. der Kompressionswellengeschwindigkeit mit der Wärmeleitfähigkeit zu korrelieren. Diese berechneten Regressionslinien stellen die Grundlage für die Erstellung eines „Wärmeleitfähigkeits-Log“ im Bohrloch dar.

Am Beispiel der kontinentalen Tiefbohrung in Deutschland werden die Modelrechnungen für die Lithologien Granit/Gneis und Basalt angewandt und mit den gemessenen Daten der Wärmeleitfähigkeit verglichen. Dabei zeigt die Korrelation der Kompressionswellengeschwindigkeit mit der Wärmeleitfähigkeit eine sehr gute Übereinstimmung. Mithilfe des elektrischen Widerstandes kann nur die Lithologie Granit/Gneis ausreichend beschrieben werden, bei Basalt führt die Regression zu erhöhten Ergebnissen.

Zum Vergleich der berechneten Regressionen (aus Sonic- bzw. Resitivity-Log) wird eine „Multiple Linear Regression“ verwendet, bei der die Wärmeleitfähigkeit mithilfe von verschiedenen Logs ermittelt wird. In einem weiteren Kapitel wird die Wärmeleitfähigkeit anhand des Geometrischen-Mittel-Modells berechnet. Dabei wird der Porenraum über das Neutron-Log ermittelt und eine stark variierende Kurve ist das Ergebnis.

Am besten kann die Wärmeleitfähigkeit mit der Kompressionswellengeschwindigkeit und der Multiplen Linear Regression berechnet werden. Alle Modelle haben aber grundsätzlich das Problem die Anisotropie der einzelnen Lithologien zu erfassen, da diese zu einer großen Bandbreite der gemessenen Wärmeleitfähigkeitsdaten führt.

Abstract

In this Master thesis the relationship between the thermal conductivity and different petrophysical parameters (electrical resistivity, compressional wave velocity) are analyzed. As a basis for the various model calculations, laboratory measurements from the Department of Applied Geophysics of the Montanuniversitaet Leoben are used. In most drilling projects, core data is not available and an indirect determination of the thermal conductivity of the various layers would lead to large cost savings.

For this purpose, the laboratory measurements are separated according to different lithologies. Thereafter, a subdivision of the samples, on the basis of the pore space, is done using electrical properties. In the next step, the thermal conductivity of the rock matrix is determined under consideration of cementation factor and pore shape (aspect ratio). Now model calculations (inclusion model) can be applied to correlate the relationship between electrical properties and the compressional wave velocity with the thermal conductivity. These calculated regression lines represent the basis for modeling a "thermal conductivity log" in the borehole.

Using the example of the continental deep drilling project in Germany the model calculations for the lithologies granite/gneiss and basalt are applied and compared with the measured data of the thermal conductivity. Correlation of the compressional wave velocity model with the thermal conductivity shows a very good agreement. The electrical resistivity model only can describe the lithology granite/gneiss adequately. For Basalt, the regression leads to increased results.

For comparison of the calculated regressions (from Sonic- and Resistivity log) a "Multiple Linear Regression" is used, in which the thermal conductivity is determined using various logs. In another chapter, the thermal conductivity is calculated from the geometric-mean model. Here, the pore space is determined with the neutron log and a very jagged curve is the result.

The best fit for thermal conductivity calculation give the compression wave velocity model and the multiple linear regression. A problem for all models, which has to be kept in mind, is the anisotropy of rocks. This effect leads to a wide range of the measured thermal conductivity data.

Table of Content

1. Introduction 1

1.1. Objectives 2

2. Geological setting KTB 3

3. Methodology 4

3.1. Thermal conductivity λ 4

3.2. Electrical properties 5

3.3. Compressional wave velocity v_p 6

3.4. Density and porosity 7

3.4.1. Density (ρ_b) 7

3.4.2. Porosity (Φ) 8

4. Model calculation 9

5. Results (lab data and models) 14

5.1. Granite/Gneiss 15

5.2. Phyllite 16

5.3. Mica schist 17

5.4. Sandstone 20

5.5. Basalt 22

6. Application on log data and comparison 25

6.1. Thermal conductivity calculation out of the Sonic log 25

6.1.1. KTB - continental deep drilling project 25

6.2. Thermal conductivity estimation out of the Resistivity log 28

6.3. Comparison model results with real data 32

6.4. Histograms 38

6.5. Multiple Linear Regression 41

6.6. Geometric-mean model 43

6.7. Comparison of applied models 45

7. Conclusion 47

8. Reference list 48

Figure captions 49

Table captions 52

1. Introduction

World's population is growing rapidly each year and the demand for energy is increasing steadily. In 2012, the main part of the world primary energy supply came from oil (33.1%), natural gas (23.9%) and coal (29.9%). The so-called fossil fuels. Only 4.7 % of the total energy consumed is generated from renewable energy sources like biofuels, wind energy and solar power (British Petroleum 2013).

Energy from geothermal resources is considered regenerative and sustainable. The installed capacity worldwide increased from 5834 Megawatt (MW) in 1990 to 10898 MW in 2010 (Bertani 2012). This shows a rising trend in the geothermal sector and is a promising alternative to the non-renewable sources.

For a geothermal project the most important parameters are the heat source and the heat flow in the zone of interest in the underground. Earth internal sources are the heat flow from the earth core and heat production by radioactive decay of instable isotopes (Uranium, Thorium and Potassium). Radiation from the sun has only little influence. The quality of a geothermal field depends on the geological and petrographic key properties, which lead to a more local aspect. Relevant properties are thermal conductivity, heat capacity, fluid saturation, local radiogenic heat production and exchange properties of porous rocks (Gegenhuber 2011).

These parameters are measured in the laboratory on core data. However, cores are rare, expensive and represent only of a small area around the borehole. Therefore, additional ways to describe the petrophysical parameters can be an advantage to get data cheaper and maybe faster. Bücker & Rybach (1996) describe a method to estimate the radiogenic heat production from gamma ray logs. Hartmann, Rath & Clauser (2005) calculated empirical relationships of thermal conductivity with compressional wave velocity and density taken from laboratory and logging data. Gegenhuber (2011) describes a "petrographic-coded model", where thermal conductivity is correlated with other petrophysical parameters under consideration of the mineral composition of the rocks. Also Fuchs (2013) made a well-log based prediction of the thermal conductivity of clastic-, carbonate- and evaporate rocks in the North German Basin.

1.1. Objectives

The main task of this thesis research is to calculate a model that can describe the thermal conductivity retrieved from logging data. For this reason a laboratory data set from the Department of Applied Geophysics of the Montanuniversitaet Leoben is used.

The research is aimed to achieve the following objectives:

1. Sort the data based on mineral composition and split it into the following groups:
   - Granite/Gneiss;
   - Phyllite;
   - Micaschist;
   - Sandstone;
   - Basalt.
2. With respect to the mineral composition, petrophysical parameters are calculated and a model for each rock type is defined. Next, the respective models are applied on the Log data to determine a fast evaluation of the thermal conductivity in boreholes.

2. Geological setting KTB

Figure 1 shows the local position of the KTB (Kontinentale Tiefbohrung, Oberpfalz) in Germany.

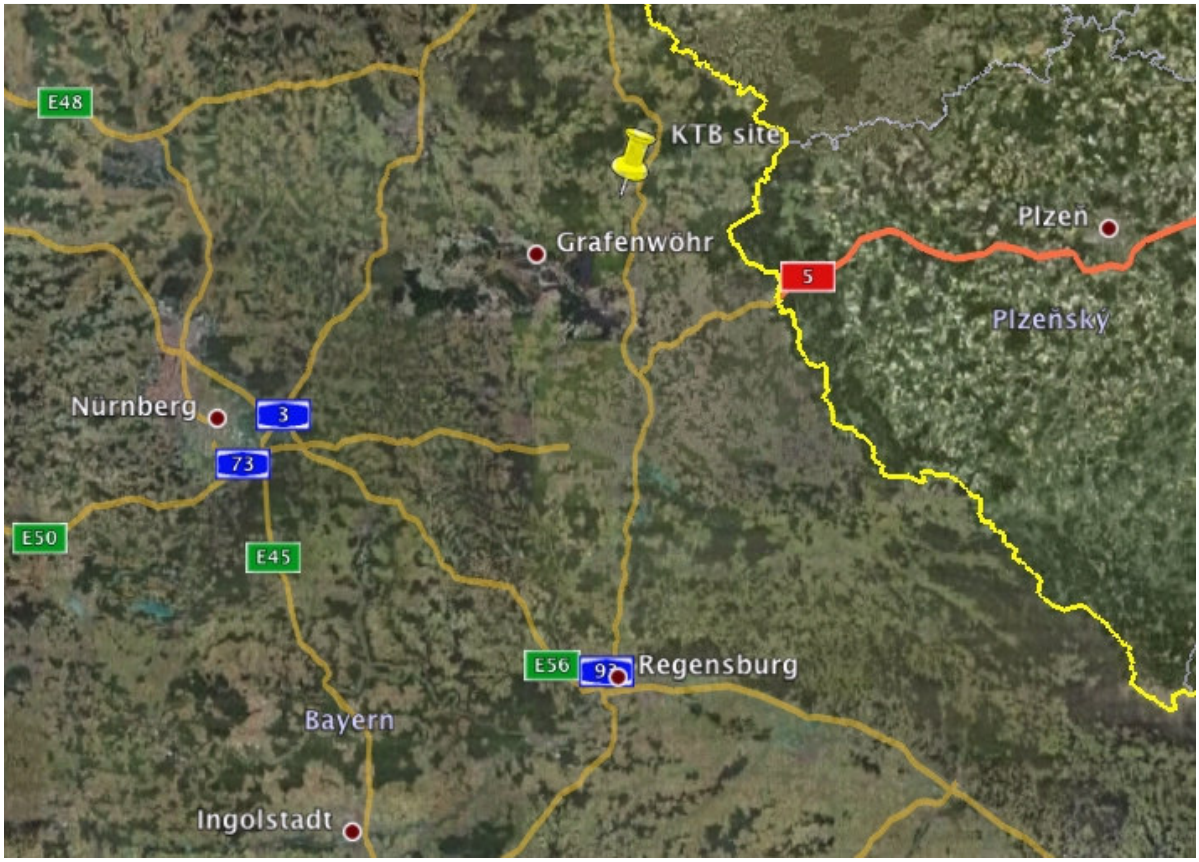

Figure 1: Geographic position KTB-Germany (GEODIS Brno, 2008)

The KTB is positioned at the boundary between the Saxothuringian and Moldanubian near the Windischeschenbach. This two formations are tectonostratigraphic parts of the Hercynian fold belt in Central Europe. Through the closure of the former oceanic basin this boundary was formed 320 million years ago. After the closure of the ocean a continent-continent collision took place and formed the mountain chain. Because of erosion the high mountain relief is sharpened and rocks, once deeply buried, appear at the surface (GeoForschungsZentrum Potsdam 2015).

The main lithologies are metabasite and gneiss. The well is explored very well and nearly every available log is made. Additionally core data is available for section down to 4000 meter.

All used data is still available on the internet (www.icdp-online.org/sites/ktb/welcome.html; Date: 17.6.2015)

3. Methodology

The laboratory measurements on numerous plugs follow the measuring methods described by Gegenhuber (2011). As part of this thesis only the calculations are performed.

3.1. Thermal conductivity λ

Thermal conductivity depends on the heat flow density q and the temperature gradient grad*T*. This is related to Fourier´s Law of thermal diffusion.

$$q = -\lambda * gradT$$

The SI unit is $Wm^{-1}K^{-1}$ (Schön 2011).

Thermal conductivity depends on (Schön 2011):

- Mineral composition: An increase of quartz content leads to an increase of thermal conductivity. Ore minerals have high values and mica minerals (Biotite) have low values of thermal conductivity;
- Temperature and pressure;
- Porosity and pore filling.

Igneous rocks show high thermal conductivity for acid or felsic and lower values for basic or mafic rocks. In sedimentary rocks the quartz content is essential. Sandstones therefore have higher values than carbonates (at comparable porosity) (Schön 2011). Metamorphic rocks show anisotropy in their thermal conductivity parallel and perpendicular to the schistosity (Gegenhuber & Schön 2010). Vosteen & Schellschmidt (2003) describe a decrease of thermal conductivity if the temperature increases.

Measuring method

The thermal conductivity is determined with a non-steady state (transient) method. The tool TK04 (from TeKa, Berlin) is used for the measurements.

As heat source (energy is defined) serves a needle encased in a cylinder (half-spaced line-source). In the middle of the needle a sensor measures the temperature as a function of time. The needle is pressed onto the sample with 15 bar and a contact agent (“Nivea” cream) is used to establish an optimal heat flow.

At the measurement a defined heating power (here: 3 Wm^{-1}) is used. The thermistor in the middle of the needle measures the temperature as a function of time. One heating period is defined with a duration of 80 seconds and 99 measurements can be taken at maximum. In the end, a heating/cooling cycle is recorded and analyzed. To consider an anisotropic effect the needle is rotated in 45° steps for each measurement.

3.2. Electrical properties

Specific electrical resistivity ρ (unit is ohm m) and its reverse the electrical conductivity (unit is Siemens/meter) are intrinsic material properties.

The electrical resistivity of rocks is controlled by the rock type, porosity permeability kind of fluid content, clay content and metallic content. The most rock forming minerals (e.g. quartz, amphibole, albite) show high resistivity. The resistivity is comparable in dry rocks, but conductivity rises in saturated, porous rocks because of electrolytic conductivity and solid fluid interactions (Schön 2011). For clean sands Archie´s Equations (Archie 1942) describe the connection of water resistivity, rock resistivity, porosity and water saturation. If the considered rocks contain clay or other conductive phases Archie´s Equations are not valid.

Measuring method

To determine the specific electric resistivity a 4-point-light instrument (Type: LF 325 from WTW, Germany) is used. The saturated one-inch-plugs are wrapped up in Teflon paper to prohibit parallel bypassing of the current outside the sample. Electrodes A and B are the source for the current. The M-, N electrodes measure the voltage as potential difference between the two ends of the cylindrical sample.

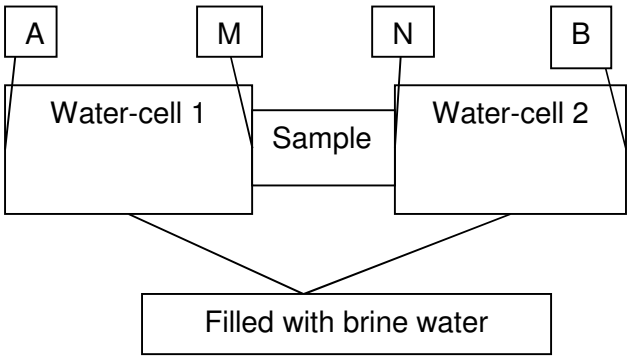

Figure 2: 4-point-light instrument

The specific electrical resistivity ρ is calculated with the following two equations:

$$\rho = k * R$$

$$R = \frac{U}{I}$$

k	geometry factor [m]	U	voltage [V]
R	resistivity [ohm]	I	current [A]

3.3. Compressional wave velocity v_p

Compressional waves (p-waves) move longitudinal in solid bodies and fluids. The velocity of the p-waves depends on the bulk modulus K, the shear modulus μ and the bulk density ρ.

$$v_p = \sqrt{\frac{K+\frac{4}{3}\mu}{\rho_b}}$$

The SI unit is m/s.

Wave velocity is related to the solid rock skeleton, the pore volume and cracks, the grain contact, pressure and temperature, the fluid saturation and the type of pore filling. The compressional wave velocity is faster in minerals than in water or gas. If the porosity increases, the velocity decreases. In metamorphic rocks anisotropy can be recognized, where the velocity parallel schistosity > perpendicular schistosity. Igneous rocks show an increase in velocity from acid to basic minerals. The velocity in sedimentary rocks is influenced by porosity the most. Unconsolidated rocks show the lowest velocity due to their grain-grain-contact and the high porosity. If the pressure increases the grain-grain-contact rises and the fractures become smaller. This effect results in higher velocities. Temperature affects the fluid and mineral properties and also the grain-grain-contact (Schön 2011).

Measuring method

The velocity of the compressional wave is determined with the first arrivals. To measure this first arrival, a “self-made” ultrasonic device (Figure 3) of the Department for Applied Geophysics was used.

At the start the sample plug (diameter = 1 inch) is fixed in the device at a pressure of 5 bar. A transmitter produces an elastic pulse moving through the sample plug and recording at the receiver. If there is no plug between the measuring adapters the dead time can be measured. To get a good connection between the sample and the measuring adapters a contact agent is used. The measured amplitudes are recorded and saved on the computer using the program “Cleverscope”. To pick the first arrivals and calculate the velocity a self-written program is applied.

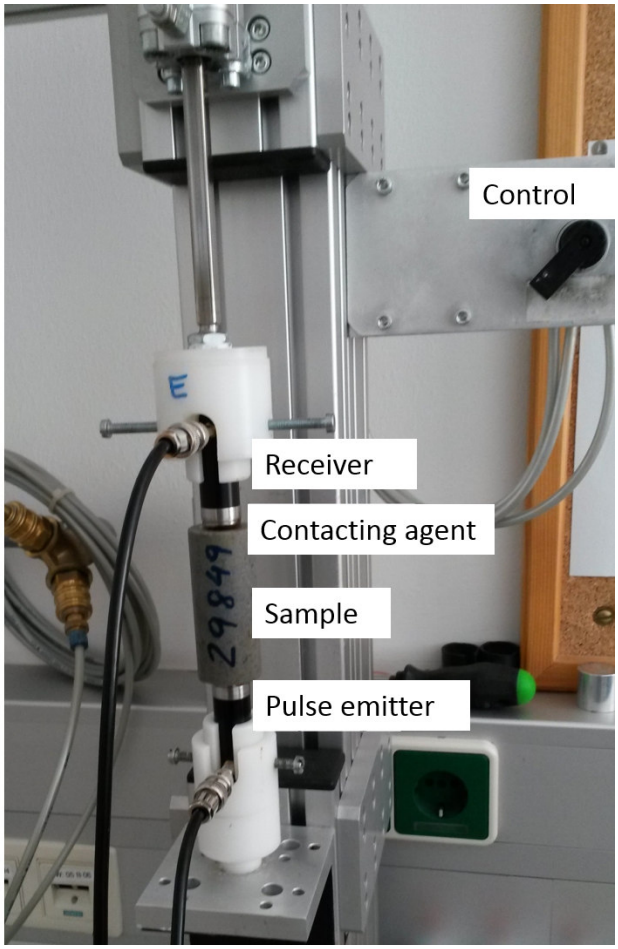

Figure 3: Ultrasonic measurement tool

3.4. Density and porosity

3.4.1. Density (ρ_b)

Density is the mass (m) in a defined volume (V):

$$\rho_b = \frac{m}{V}$$

The SI unit is kg/m³ or g/cm³.

It has to be distinguished between:

- ρ_b bulk density
- ρ_i density of a component of the rock, e.g. quartz (2,648 g/cm³)
- ρ_s matrix density
- ρ_{fl} fluid density

A typical bulk density of granite ranges between 2.50 and 2.80 g/cm³. (Schön 2011)

3.4.2. Porosity (Φ)

Porosity describes the existing fluid store volume of rocks (water, oil, gas) and influences a lot of rock specific parameters, e.g. the density. It is important to distinguish between total porosity and effective porosity. The effective porosity considers the connected pores only (Schön 2011).

$$total\ porosity\ \Phi_{total} = \frac{V\ pores}{V\ total}$$

$$effective\ porosity\ \Phi_{eff} = \frac{V\ connected\ pores}{V\ total}$$

Measuring method:

The grain density is determined with a helium pycnometer. The volume of solid objects can be measured in the pycnometer with the ideal gas equation. With the weight of the sample the grain density can be calculated.

The effective porosity is determined with the principle of Archimedes, where the sample is weighted dry, saturated and under buoyancy.

4. Model calculation

Thermal conductivity depends mainly on mineral composition and porosity or fractures. In this study, laboratory data is compared with calculated data in different steps. To link the matrix and fluid properties the inclusion model after Budiansky & O'Connell (1976) (elastic properties) and Clausius-Mossotti (thermal properties) are used. To calculate the formation factor the model after Archie (1942) is applied.

The model calculation is explained with the lithology granite/gneiss.

To sort different lithologies, on the basis of their pore space, electrical properties are used. These properties are available from borehole measurements and from laboratory data most of the time. The formation factor (F) is independent from rock type (all rock building minerals are isolators). Just the shape of the pore space has an influence on this parameter (and of course the pore filling). For this reason the measured formation factor and the porosity of the samples are compared with a calculated formation factor F after Archie (1942).

$$F = \frac{1}{\Phi^m} = \frac{R_0}{R_w}$$

m… cementation factor [ ] R_0… resistivity formation [ohm m]

Φ… effective porosity [ ] R_w… resistivity water [ohm m]

F… formation factor [ ]

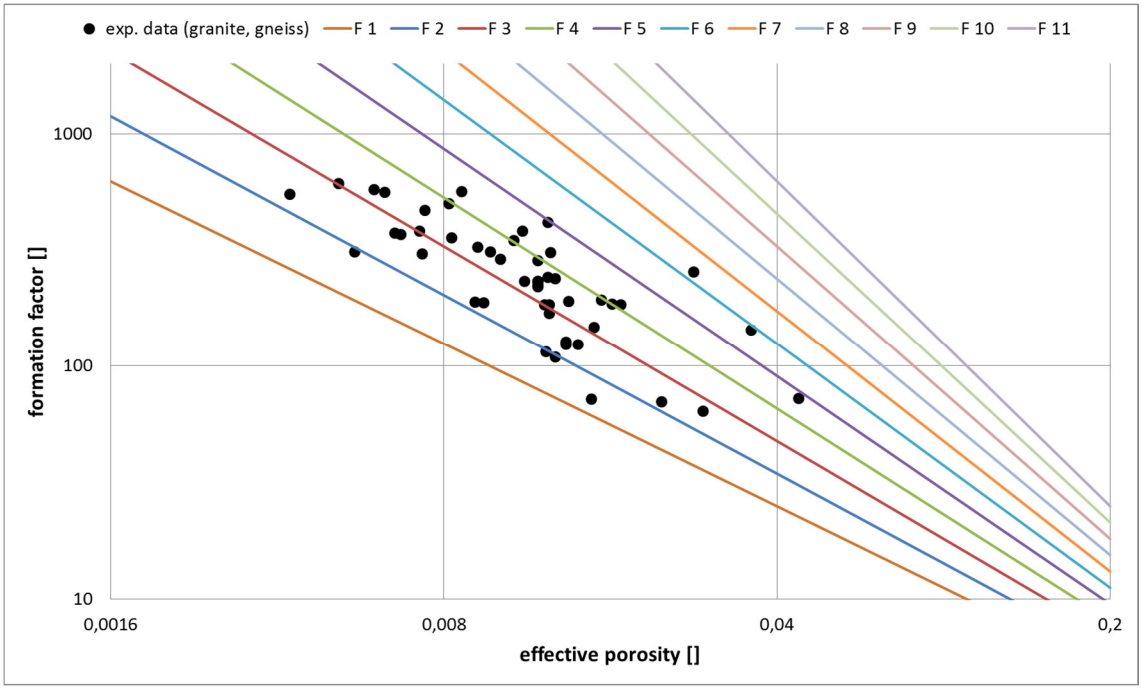

Figure 4: Formation factor vs. effective porosity (points= experimental data, lines= calculated data from F1 (m=1) to F11 (m=2))

Figure 4 indicates the correlation of formation factor with effective porosity. The lines are calculated with the porosity and cementation factor after Archie (1942), the experimental data is evaluated with the electrical resistivities.

Samples with a low cementation factor show flat or jointed pores. Spherical pores show a higher cementation factor.

The inclusion model estimates penny-shaped pores and therefore Budiansky & O'connell (1976) developed equations for the elastic properties:

$$k_{SC} = k_S * [1 - \frac{16}{9} * \frac{1 - v_{SC}^2}{1 - 2v_{SC}} * \varepsilon]$$

$$\mu_{SC} = \mu_s * [1 - \frac{32}{45} * \frac{(1 - v_{SC}) * (5 - v_{SC})}{2 - v_{SC}} * \varepsilon]$$

k_{sc}... calculated bulk modulus k_s… bulk modulus host material

μ_{sc}… calculated shear modulus μ_s… shear modulus host material

Bulk and shear modulus of the host material are determined from laboratory measurements by plotting the bulk or shear modulus versus the porosity and only samples, which have a very low porosity (below 0.015 for granite and 0.01 for other lithologies) are considered. A linear trend is calculated and 30% is added to the value at 0% porosity (Figure 5 and Figure 6). The addition of 30% is used because in this case the higher pressures and temperatures in depth, which lead to a higher bulk- and shear modulus, are considered.

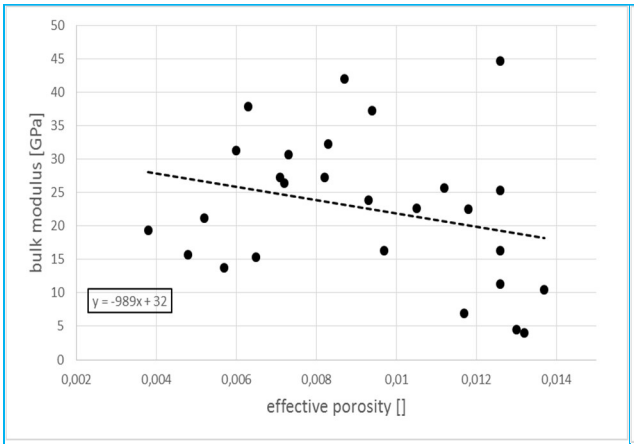

Figure 5: Bulk modulus determination (granite/gneiss)(experimental data with linear regression)

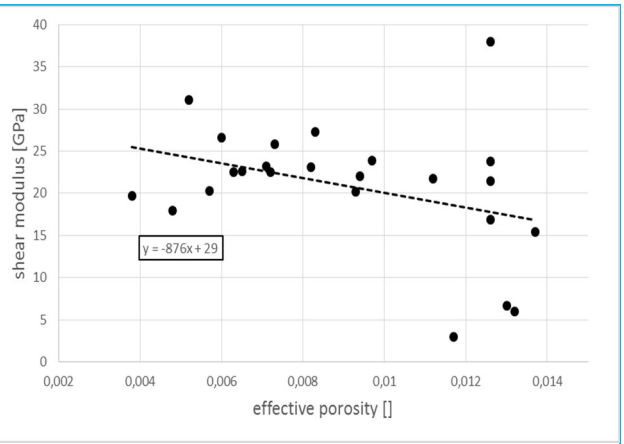

Figure 6: Shear modulus determination (granite/gneiss)(experimental data with linear regression)

ε… crack density parameter (Mavko, Mukerji & Dvorkin, 2009)

$$\varepsilon = \left(\frac{\Phi}{\alpha}\right) * \left(\frac{3}{4\pi}\right)$$

α… aspect ratio (α=a/c)

v_{sc}… effective Poisson´s ratio (Mavko, Mukerji & Dvorkin, 2009)

$$v_{SC} \approx v_S * [1 - \frac{16}{9} * \varepsilon]$$

v_s... Poisson ratio host material

To calculate the velocity of the compressional wave v_p also the bulk density ρ_b is needed:

$$\rho_b = (1 - \Phi) * \rho_s + \Phi * \rho_{air}$$

$$v_p = (\frac{k_{SC} + \frac{4}{3} * \mu_{SC}}{\rho_b})^{1/2}$$

ρ_s… grain density (mean value experimental data)

ρ_{air}… density air (=0.0012 [g/cm³])

The thermal conductivity is calculated with the equation of Clausius-Mossotti (Berryman 1995):

$$\lambda_{CM} = \frac{1 - 2 * \phi * R_{mi} * (\lambda_S - \lambda_{fl})}{1 + \phi * R_{mi} * (\lambda_S - \lambda_{fl})}$$

$$R_{mi} = \frac{1}{9} * (\frac{1}{L_{a,b,c} * \lambda_{fl} + (1 - L_{a,b,c}) * \lambda_S})$$

λ_S… thermal conductivity matrix

λ_{fl}… thermal conductivity inclusion

R_{mi}… function of depolarization exponents L_a, L_b, L_c

In this study the shape of the pores are idealized as plate-like objects (a=b>>c) which follow the calculations of Sen (1981).

$$L_c = 1 - \frac{\pi}{2} * \frac{c}{a} = 1 - \frac{\pi}{2} * \alpha$$

$$L_a = L_b = \frac{1 - L_c}{2} = \frac{\pi}{4} * \alpha$$

Table 1 gives an overview of aspect ratios and the resulting depolarization factors.

α	La=Lb	Lc
0,02	0,0157	0,9686
0,01	0,0079	0,9843
0,003	0,0024	0,9953

Table 1: Aspect ratios and resulting depolarization factors

The thermal conductivity of the matrix λ_S is determined by plotting the thermal conductivity versus the effective porosity (Figure 7). To eliminate the influence of pores, thermal conductivity is modeled (Clausius-Mosotti) under consideration of different aspect ratios. The experimental data should range between the higher and the lower aspect ratio. The point at 0 porosity shows λ_s.

The laboratory data is colored on the basis of their cementation factor m. In this way a correlation between the aspect ratio and the cementation factor can be made. Samples with low cementation factor should have a lower aspect ratio.

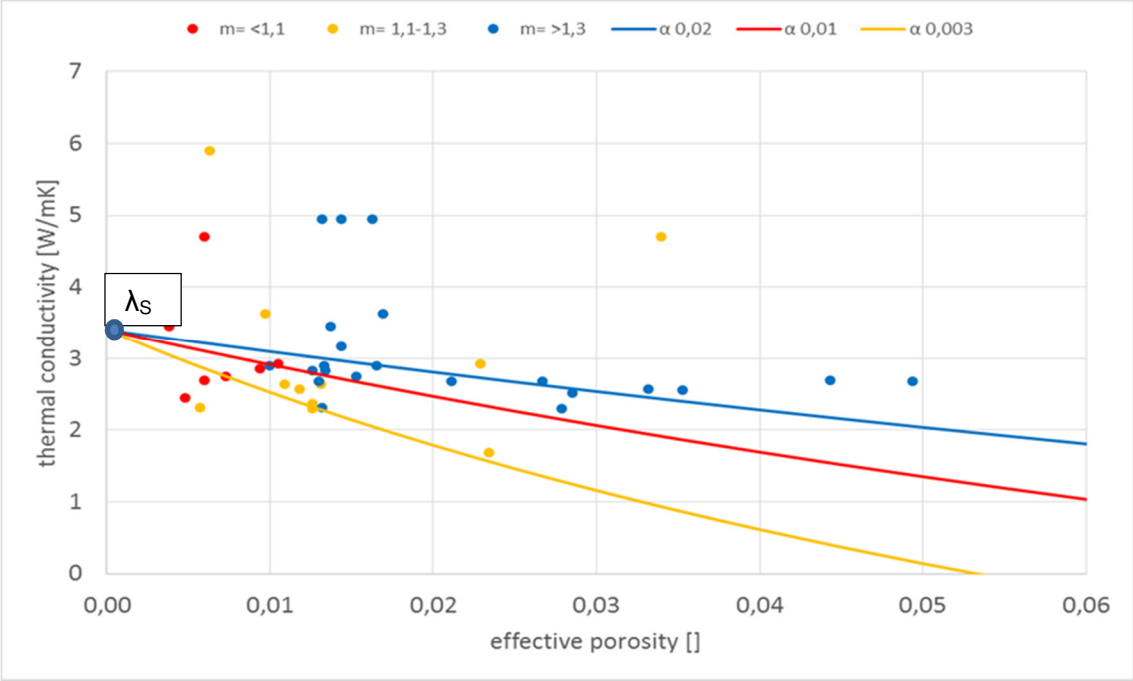

Figure 7: Thermal conductivity vs. effective porosity (points=experimental data sorted after cementation factor m, lines= calculated data with different aspect ratio α)

In the next step the formation factor is plotted with the thermal conductivity (Figure 8). This diagram should provide an overview how strong the thermal conductivity is affected by the form of the pores. The plotted lines describe the calculated thermal conductivity (Clausius-Mossotti) and the calculated formation factor ($F=1/\Phi^m$). For a low aspect ratio also a low cementation factor is expected. If the curves characterize the experimental data significantly, the shape of the pores influence the thermal conductivity a lot.

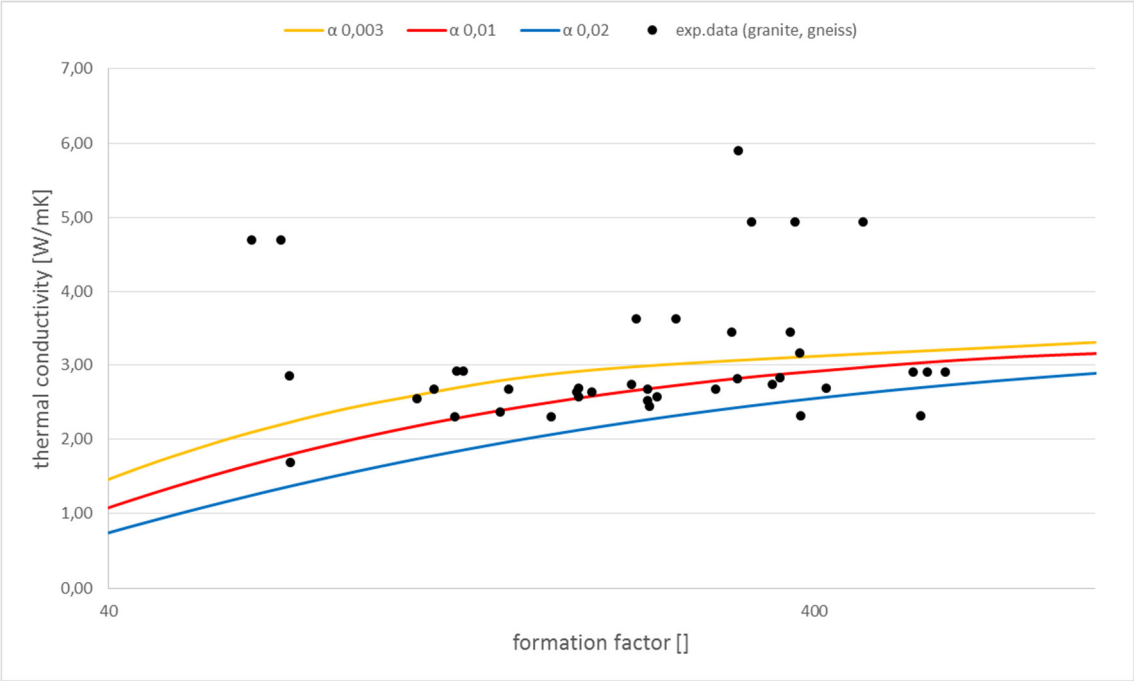

Figure 8: Thermal conductivity vs. formation factor (points=experimental data, lines=calculated data with different aspect ratios and cementation factors e.g. red line= low aspect ratio and low cementation factor)

Finally the thermal conductivity is correlated with the compressional wave velocity v_p (Figure 9). This diagram is the basis for the regression formula to estimate the thermal conductivity from the sonic log. The lines present calculated data after Clausius-Mossotti under consideration of three different aspect ratios.

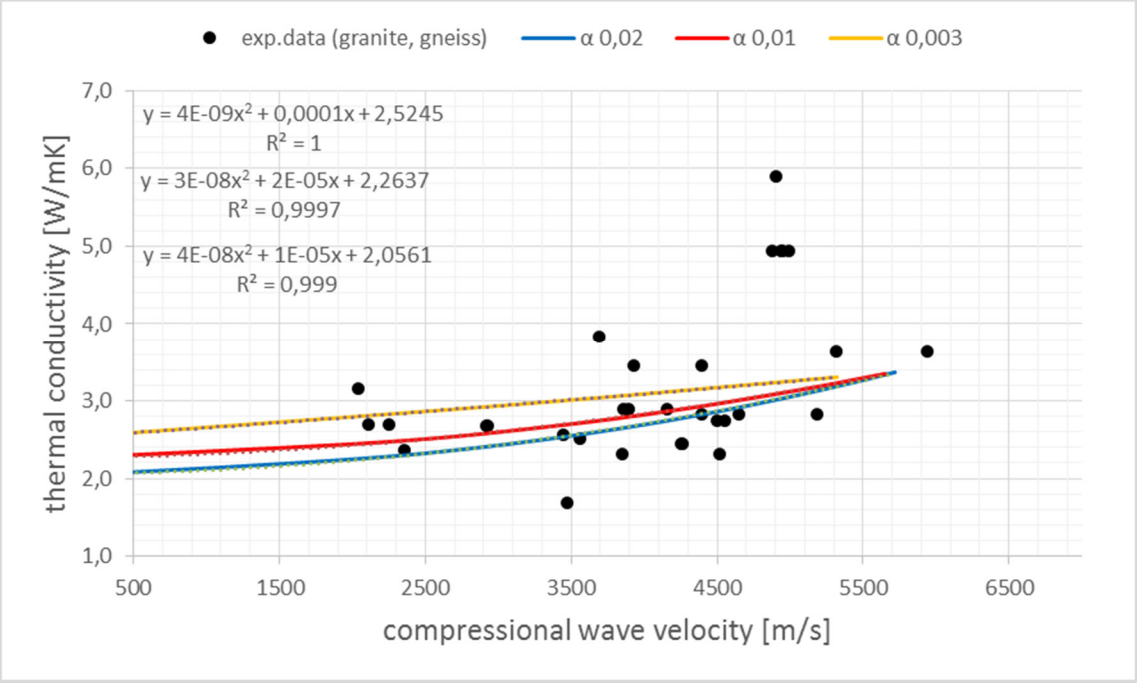

Figure 9: Thermal conductivity vs. v_p (points=experimental data, lines= calculated data with different aspect rations)

The solid properties for the calculation of granite/gneiss are:

λ_s= 4 W/mK λ_{fl}= 0,025 W/mK k_s=41 GPa μ_s=38 GPa ρ_s=2.74 g/cm³;

with a resulting velocity of the matrix $v_{p,s}$= 5784 m/s.

In order to respect the shape of the pores three aspect ratios are used:

α= 0.02: L_a= 0.0157 L_c= 0.9686 R_{mi}= 0.798

α= 0.01: L_a= 0.0079 L_c= 0.9843 R_{mi}= 1.327

α= 0.003: L_a= 0.0024 L_c= 0.9953 R_{mi}= 2.596

5. Results (lab data and models)

The model calculations are used for 5 different lithologies. For every lithology the properties of the host rock are determined with the laboratory data and they build the basis for the calculations.

Table 2 gives an overview of the input data for the inclusion model for the different lithologies.

		Granite, Gneiss	Phyllite	Mica schist	Sandstone	Basalt
λs	**[W/mK]**	3.4	4	4.3	4.2	3.2
λi	**[W/mK]**	0.025	0.025	0.025	0.025	0.025
ks	**[GPa]**	41	72	62	43	108
μs	**[GPa]**	38	42	49	39	89
υs	**[GPa]**	0.146	0.256	0.187	0.152	0.177
ρs	**[g/cm³]**	2.74	2.79	2.77	2.73	2.98
ρair	**[g/cm³]**	0.0012	0.0012	0.0012	0.0012	0.0012
vp,solid	**[m/s]**	5784	6773	6780	5899	8741
α1	**[]**	0.02	0.02	0.02	0.03	0.02
α2	**[]**	0.01	0.01	0.01	0.01	0.005
α3	**[]**	0.003	0.003	0.0015	0.004	0.001
m1	**[]**	1	1	1	1	1
m2	**[]**	1.3	1.3	1.35	1.35	1.25
m3	**[]**	1.7	1.75	1.9	1.8	1.8

Table 2: Overview of the host properties and assumed aspect ratios for different lithologies

5.1. Granite/Gneiss

The first considered lithology is granite/gneiss. Figures for interpretation are shown in the section before (4. Model calculations).

All samples in Figure 4 have a porosity below 5 % and the cementation factor m ranges between 1 and 1.5. This indicates a low range of the cementation factor and therefore flat or jointed pore spaces are expected.

Figure 5 and Figure 6 show the determination of the shear and bulk modulus. The linear regression for the bulk modulus points out a value of 32 GPa and for the shear modulus 29 GPa. Tests show that the best fit in the calculations occur if 30% are added to this values, so the used Bulk modulus is 41 GPa and the used shear modulus is 38 GPa.

The thermal conductivity of the matrix λ_S is set at 3.4 W/mK. In this way the curves correlate the best with the experimental data (Figure 7). Also the correlation of the aspect ratio with the cementation factor is plotted in Figure 7. Samples with a low cementation factor fit the low aspect ratio curve and samples with higher cementation factor fit the high aspect ratio curve well. Few samples show higher thermal conductivity and don´t fit to the curves. A different mineral composition (e.g. high quartz content) could be the reason. Another reason is the effect of anisotropy. The samples with the high thermal conductivity are so-called “Flaser gneisses” (layered texture) and “Migmatit” and therefore a high thermal conductivity can be measured parallel to the texture.

Figure 8 shows the thermal conductivity versus the formation factor. The curves fit the experimental data very well. This indicates a strong link between the thermal conductivity and the shape of the pores. Again a few values don´t correlate with the calculated data because of a different mineral composition and anisotropy. The formation factor for the curves is calculated with m=1 for the low aspect ratio, m=1.3 for the medium and m=1.7 for the high aspect ratio.

Figure 9 is the most important diagram because the regressions will be used for thermal conductivity estimation out of borehole logs. The compressional wave velocity shows similarities with the thermal conductivity, because both depend on mineral composition, the shape of pores and their filling. The model works well to describe the laboratory data. The aspect ratio for best fit is 0.02. Overall the thermal conductivity of the samples varies between 2.2 W/mK and 3.8 W/mK.

Only 4 samples are outliers with a higher thermal conductivity and one sample has a very low value. This is the effect of anisotropy and the direction of measuring the sample parallel or perpendicular to the texture. Also the mineral composition has a high influence.

Table 3 presents the resulting regression equations for the lithology.

Rocktype	aspect ratio	Regression equations	R^2
Granit/Gneiss	0.003	$\lambda=4E\text{-}09*v_p^2+0.0001*v_p+2.52$	1
Granit/Gneiss	0.01	$\lambda=3E\text{-}08*v_p^2+2E\text{-}05*v_p+2.26$	0.999
Granit/Gneiss	0.02	$\lambda=4E\text{-}08*v_p^2+1E\text{-}05*v_p+2.06$	0.999

Table 3: Regressions and coefficient of determination from calculated curves for different aspect ratios (granite/gneiss) (λ in W/mK, v_p in m/s)

5.2. Phyllite

All samples have a porosity below 2 % and the cementation factor ranges between 1 and 1.35. The low cementation factor indicates flat pores like the granite/gneiss lithology.

Figure 10 is used to show the correlation between the thermal conductivity and the shape of the pores. The calculated curves fit the experimental data well in the lower area of the thermal conductivity and represent a strong connection of the thermal conductivity with the shape of the pores. Samples with a higher thermal conductivity have a higher content of chlorite and quartz. The outliers with a low formation factor are phyllites with a high content of graphite. (It is not a low porosity effect!).

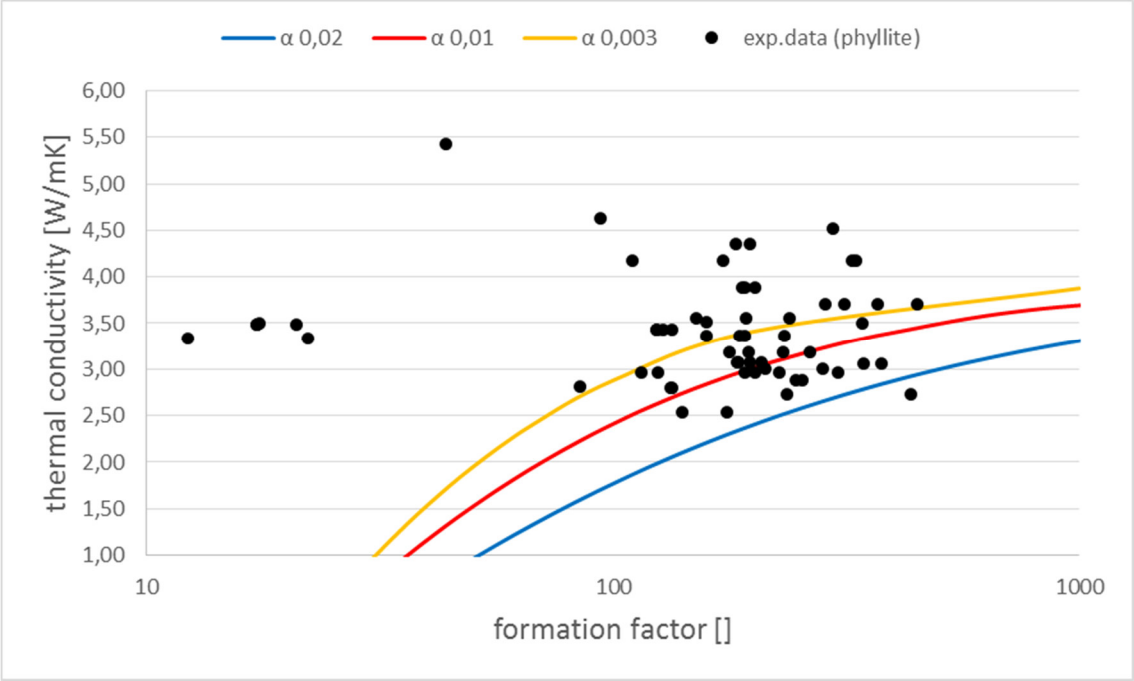

Figure 10: Thermal conductivity vs. formation factor (phyllite) (points=experimental data, curves= calculated data with different aspect ratios and cementation factors e.g. orange line= low aspect ratio and low cementation factor)

The formation factor for the curves is calculated with m=1 for the low aspect ratio, m=1.3 for the medium and m=1.75 for the high aspect ratio.

In Figure 11 the regression curves for the thermal conductivity estimation can be seen. The calculated curves fit the experimental data quite good. The experimental data has a thermal conductivity between 2.5 W/mK and 4.5 W/mK. Again the influence of the mineral composition has a high influence and also anisotropy effects the data.

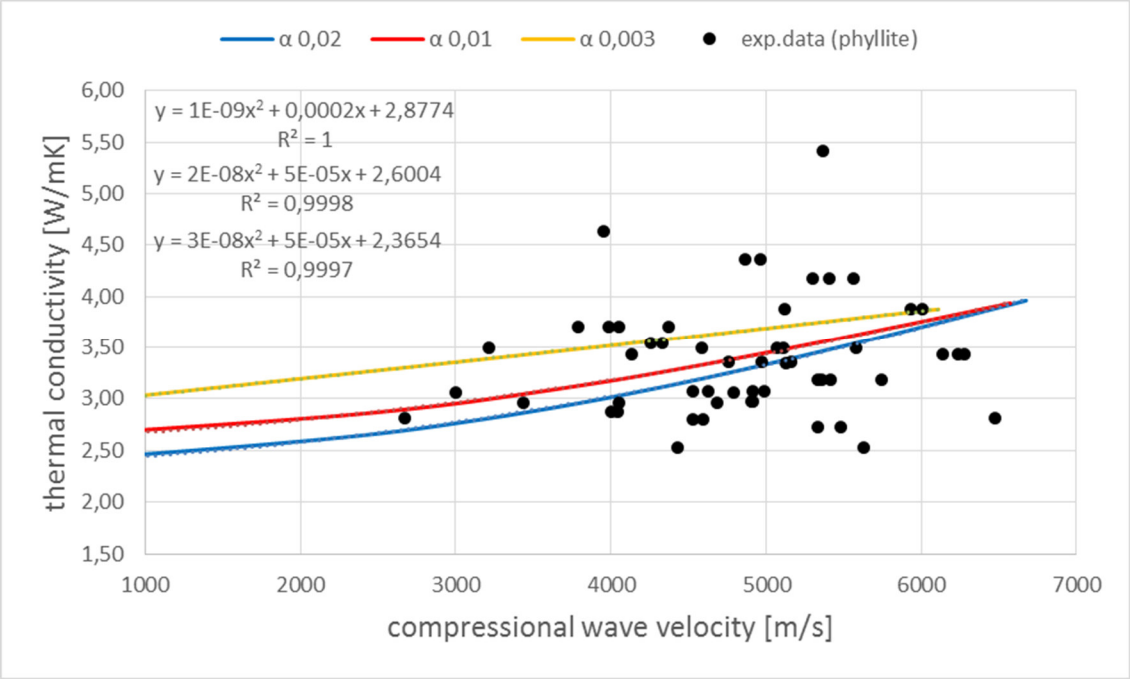

Figure 11: Thermal conductivity vs. compressional wave velocity (phyllite) (points= experimental data, curves= calculated data for different aspect ratios)

Table 4 presents the resulting regression equations for the lithology.

Rocktype	aspect ratio	Regression equations	R^2
Phyllite	0.003	λ=1E-09*v_p^2+ 0.0002*v_p + 2.88	1
Phyllite	0.01	λ=2E-08*v_p^2+ 5E-05*v_p + 2.60	0.999
Phyllite	0.02	λ=3E-08*v_p^2+ 5E-05*v_p + 2.37	0.999

Table 4: Regressions and coefficient of determination from calculated curves for different aspect ratios (phyllite) (λ in W/mK, v_p in m/s)

5.3. Mica schist

The third lithology considered is divided into 2 parts, because of the cementation factor of the samples. Mica schist 1 has a low cementation factor in the range from 1 to 1.25, so flat pores are expected. Mica schist 2 has a cementation factor between 1.25 and 1.6. Therefore more spherical pores are expected. The porosity of all samples are below 5 %.

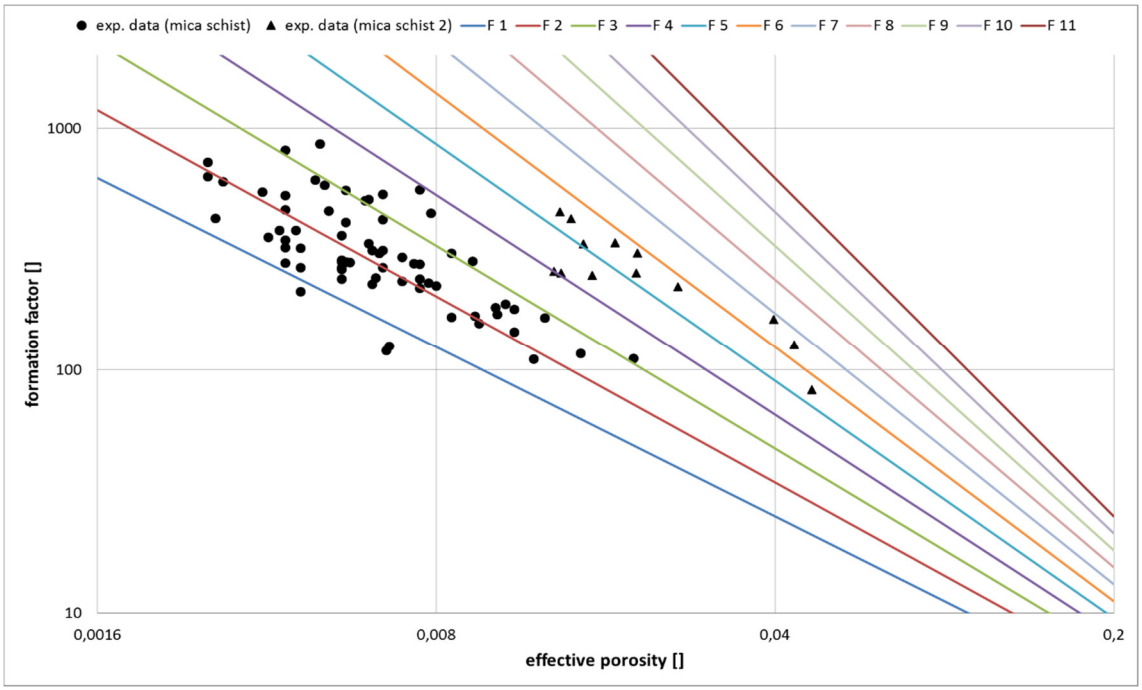

Figure 12: Formation factor vs. effective porosity (mica schist) (points, triangles= experimental data, lines= calculated data from F1 (m=1) to F11 (m=2))

Figure 13 shows the thermal conductivity versus the formation factor. Garnet has a high thermal conductivity, therefore samples with a garnet content are highlighted. The calculated curves describe the experimental data well. Again, samples with higher thermal conductivity are effected by mineral composition and anisotropy.

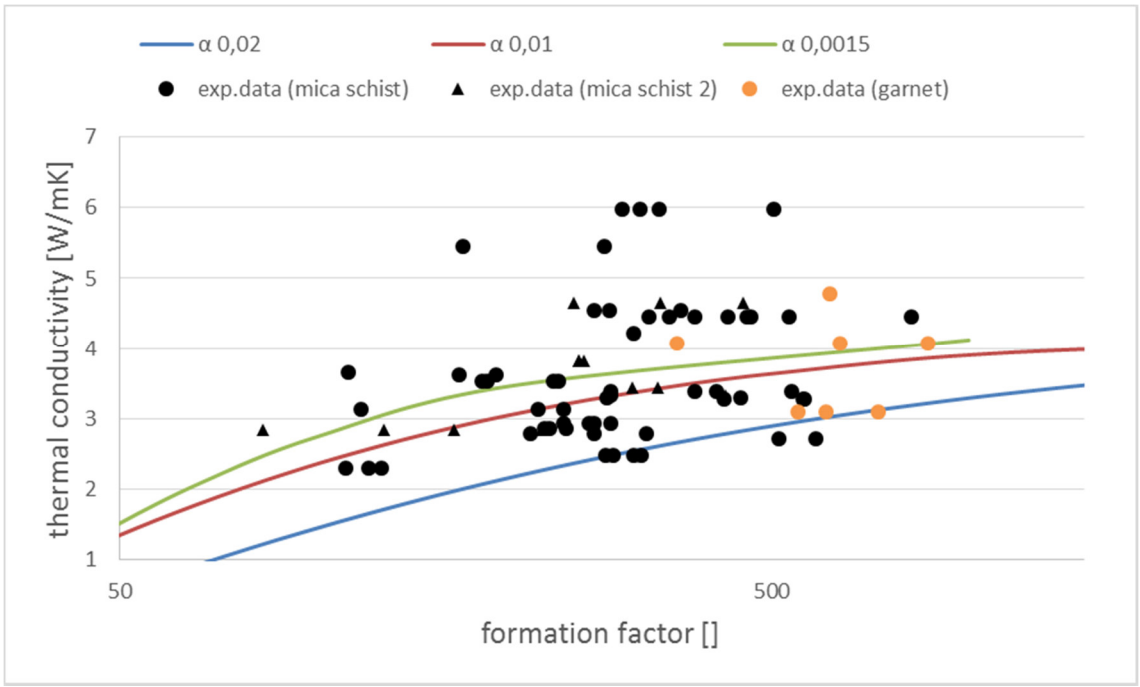

Figure 13: Thermal conductivity vs. formation factor (mica schist) (points, triangles=experimental data, curves= calculated data with different aspect ratios and cementation factors e.g. orange line= low aspect ratio and low cementation factor)

Samples with garnet don´t show a characteristic deviation of the other samples. The formation factor for the curves is calculated with m=1 for the low aspect ratio, m=1.35 for the medium and m=1.9 for the high aspect ratio.

The thermal conductivity is plotted versus v_p in Figure 14. A difference between mica schist 1 and mica schist 2 cannot be recognized. Also the samples with garnet don´t show a significant higher thermal conductivity. Samples with a high thermal conductivity (around 6 W/mK) can be described with the effect of anisotropy. There is no indication that the mineral composition has a high influence for this samples. Samples with a very low thermal conductivity (around 2.5 W/mK) have a layered texture and may be measured perpendicular to the layers. Therefore also the anisotropy effect has a high influence.

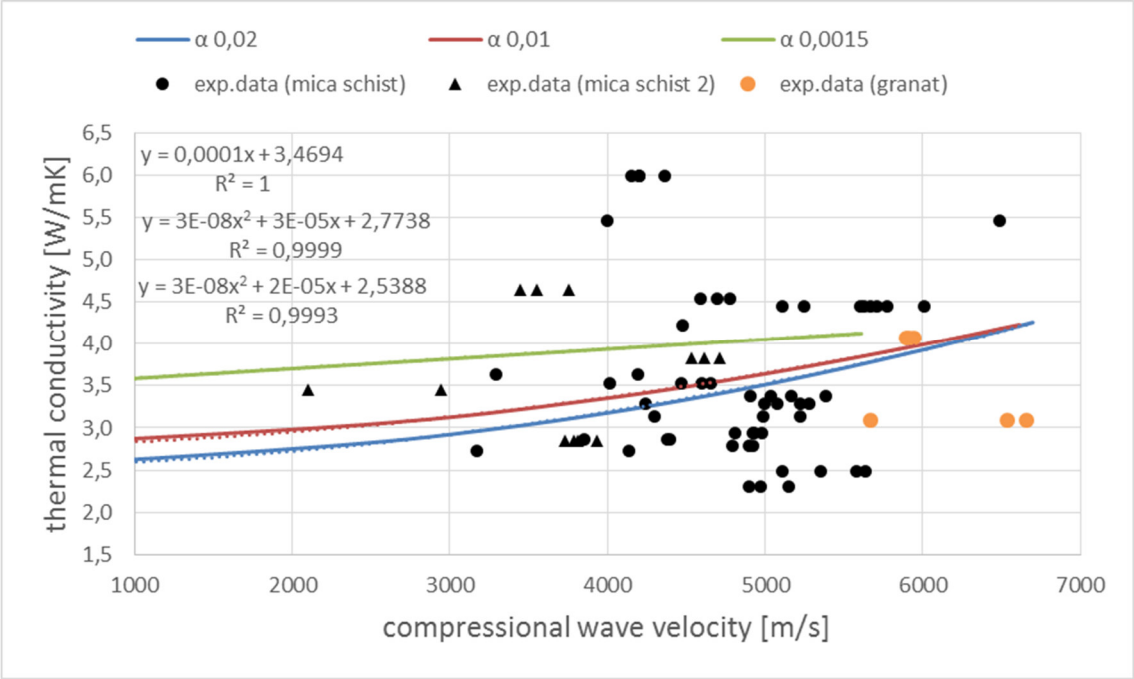

Figure 14: Thermal conductivity vs. compressional wave velocity (mica schist) (points, triangles = experimental data, curves= calculated data for different aspect ratios)

Table 5 presents the resulting regression equations for the lithology.

Rocktype	aspect ratio	Regression equations	R^2
Mica schist	0.0015	$\lambda=0.0001*v_p+3.47$	1
Mica schist	0.01	$\lambda=3E\text{-}08*v_p^2+3E\text{-}05*v_p+2.77$	0.999
Mica schist	0.02	$\lambda=3E\text{-}08*v_p^2+2E\text{-}05*v_p+2.54$	0.999

Table 5: Regressions and coefficient of determination from calculated curves for different aspect ratios (mica schist) (λ in W/mK, v_p in m/s)

5.4. Sandstone

The lithology sandstone is also divided into 2 parts. Sandstone 1 has a porosity below 2 % so flat pores are expected and the cementation factor ranges between 1 and 1.25. Sandstone 2 has a porosity from 2 % to 18 %. Therefore more spherical pores are estimated and the cementation factor is between 1.3 and 1.8. Two samples have a cementation factor above 2, which indicates a highly cemented sandstone.

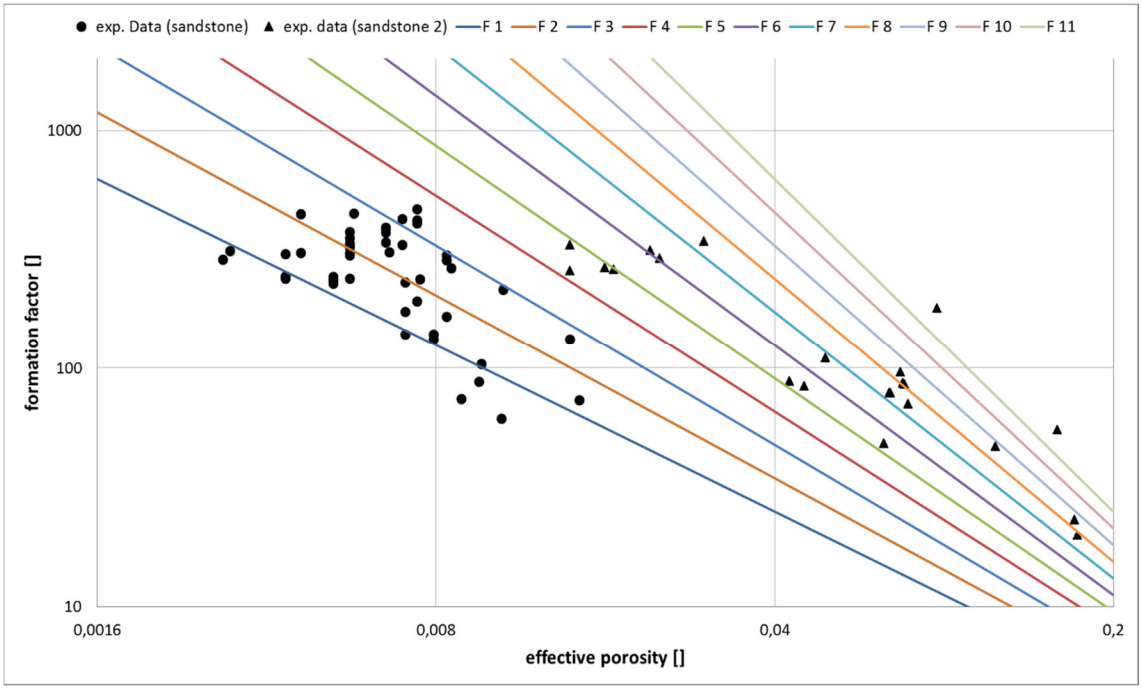

Figure 15: Formation factor vs. effective porosity (sandstone) (points, triangles= experimental data, lines= calculated data from F1 (m=1) to F11 (m=2))

The lithology sandstone shows a strong connection of thermal conductivity with the shape of the pores (Figure 16). Sandstone 2 has a significant lower thermal conductivity-formation factor ratio as sandstone 1. The three samples with a very high thermal conductivity are metaarenites. The formation factor for the curves is calculated with m=1 for the low aspect ratio, m=1.35 for the medium and m=1.8 for the high aspect ratio.

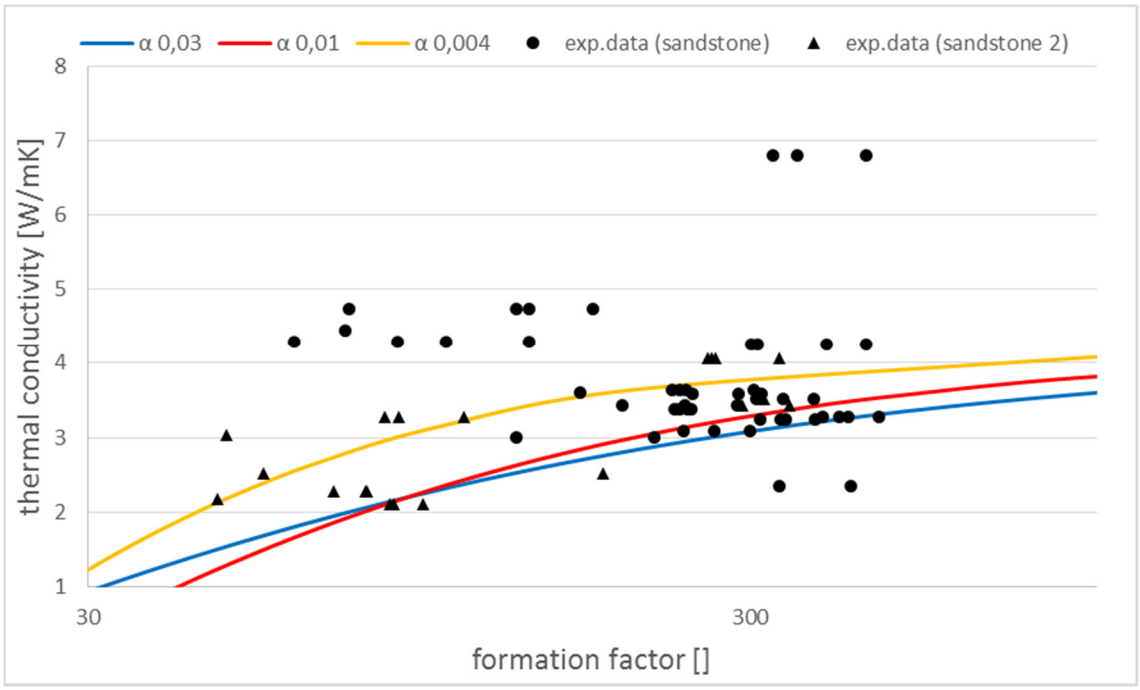

Figure 16: Thermal conductivity vs. formation factor (sandstone) (points, triangles=experimental data, curves= calculated data with different aspect ratios and cementation factors e.g. orange line= low aspect ratio and low cementation factor)

In Figure 17 the thermal conductivity is plotted versus v_p.

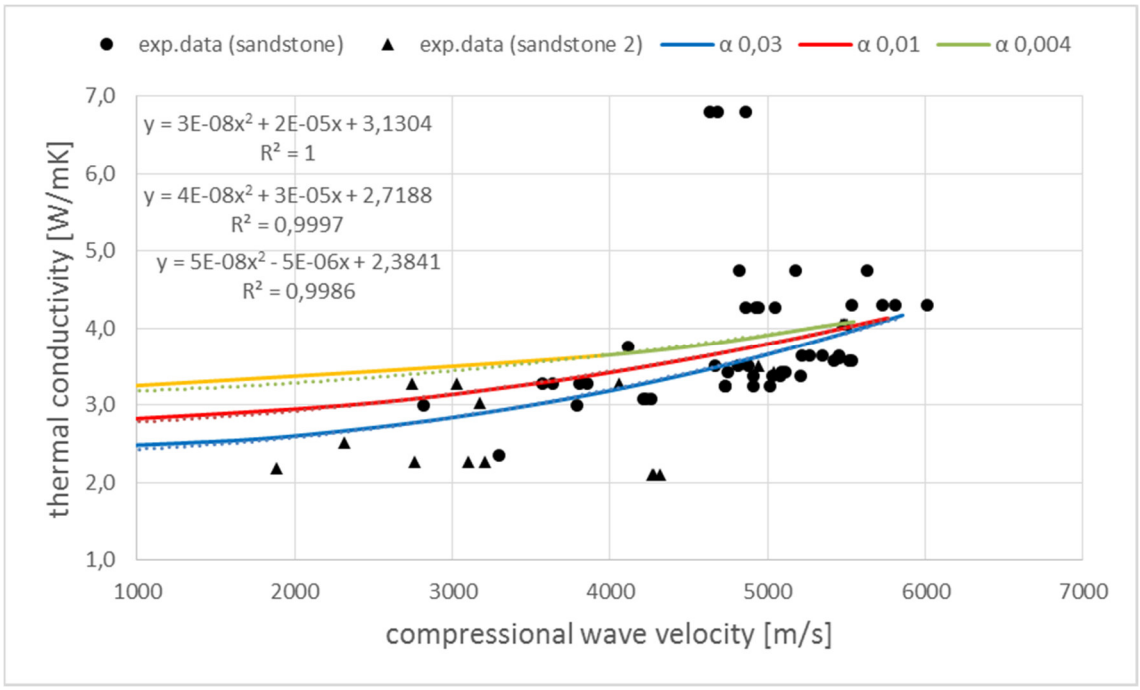

Figure 17: Thermal conductivity vs. compressional wave velocity (sandstone) (points, triangles= experimental data, curves= calculated data for different aspect ratios)

The calculated curves can describe the experimental data, but Sandstone 2 shows a slightly lower thermal conductivity as estimated. A reason could be the higher clay content of the

samples. Sandstone 2 samples with a higher thermal conductivity have a higher quartz content. Thermal conductivity of sandstone 1 ranges between 3 W/mK and 5 W/mK (3 outliers).

Table 6 presents the resulting regression equations for the lithology.

Rocktype	aspect ratio	Regression equations	R^2
Sandstone	0.004	$\lambda=3E\text{-}08*v_p^2 + 2E\text{-}05*v_p + 3{,}13$	1
Sandstone	0.01	$\lambda=4E\text{-}08*v_p^2 + 3E\text{-}05*v_p + 2.72$	0.999
Sandstone	0.03	$\lambda=5E\text{-}08*v_p^2 + 5E\text{-}06*v_p + 2.38$	0.999

Table 6: Regressions and coefficient of determination from calculated curves for different aspect ratios (sandstone) (λ in W/mK, v_p in m/s)

5.5. Basalt

The lithology basalt is divided into two parts. All samples of basalt 1 have a porosity below 3 % and the cementation factor m ranges between 1 and 1.3. This indicates a low range of the cementation factor and therefore flat or jointed pore spaces are expected. Samples of basalt 2 have a porosity between 6 % and 14 % and a cementation factor higher than 1.7 which indicates spherical pores (Figure 18).

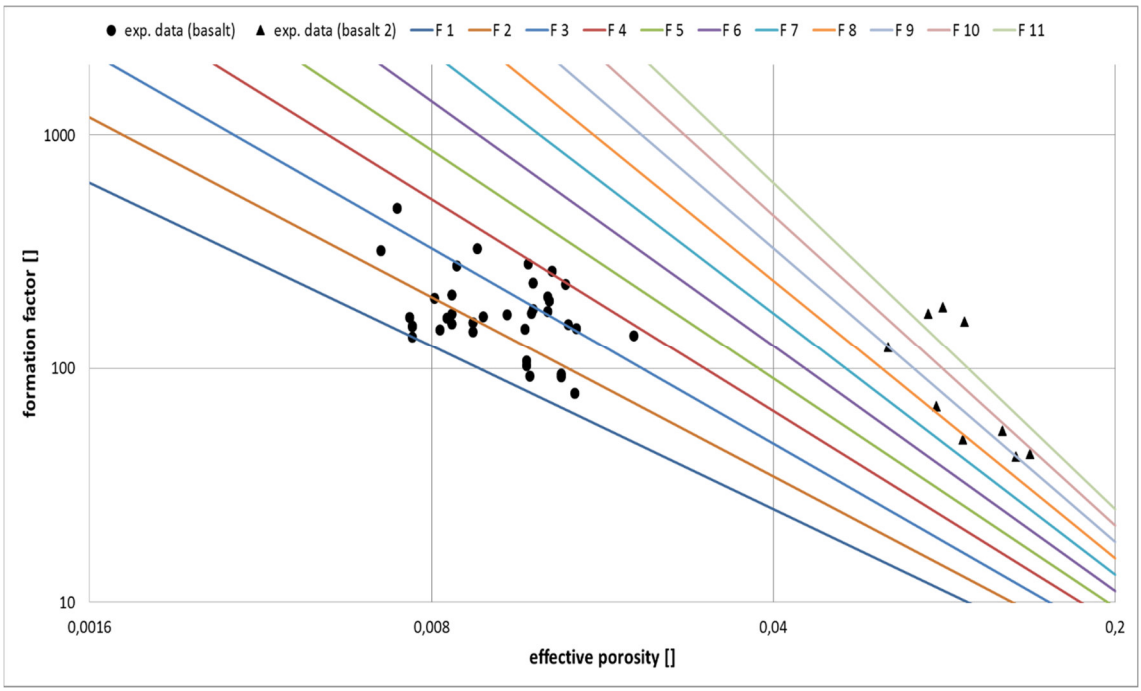

Figure 18: Formation factor vs. effective porosity (basalt) (points, triangles= experimental data, lines= calculated data from F1 (m=1) to F11 (m=2))

Figure 19 shows the thermal conductivity versus the formation factor for basalt 1 (For basalt 2 no experimental data of the thermal conductivity was available.). The experimental data varies very much so the calculated curves can only describe a part of it. This indicates that the link between the thermal conductivity and the shape of the pores is not very strong. High and low

thermal conductivity values don´t correlate with the calculated data because of a different mineral composition and anisotropy. Samples with a low value are amphibolites with a scheelite content. Samples with a high geothermal conductivity are meta-basites. The formation factor for the curves is calculated with m=1 for the low aspect ratio, m=1.25 for the medium and m=1.8 for the high aspect ratio.

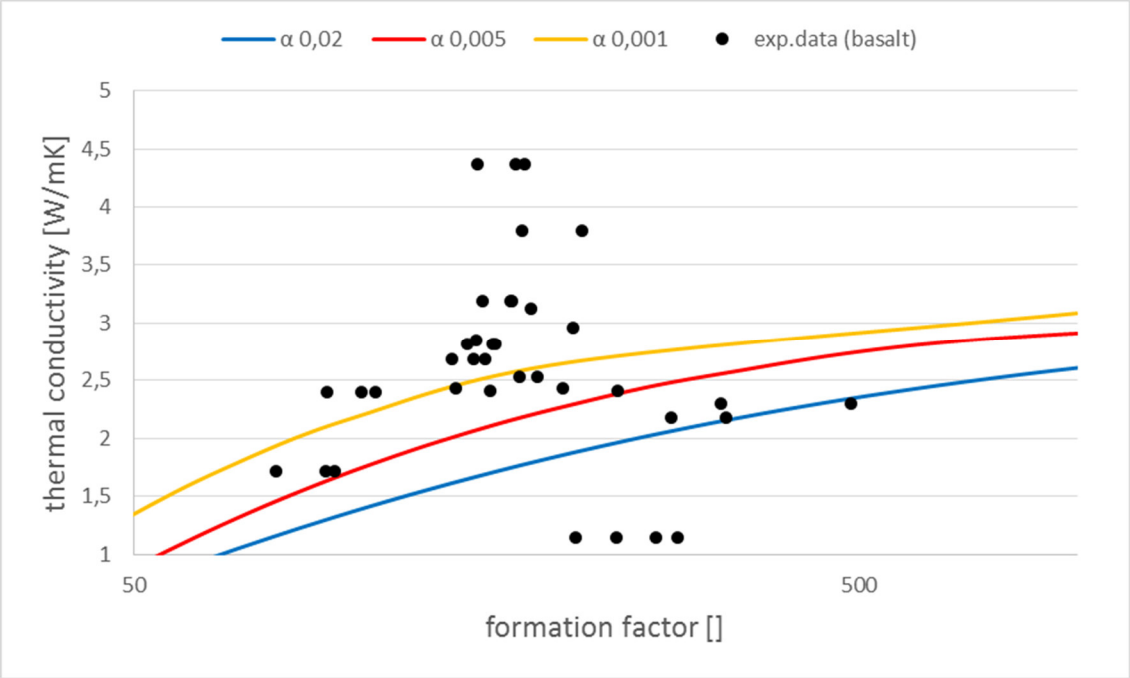

Figure 19: Thermal conductivity vs. formation factor (basalt 1) (points =experimental data, curves= calculated data with different aspect ratios and cementation factors e.g. orange line= low aspect ratio and low cementation factor)

The thermal conductivity is plotted versus v_p in Figure 20. The calculated curves can describe the experimental data fairly, but the measured data scatters too much. Samples with a very low thermal conductivity are effected by mineral composition (scheelite, amphibolite) and anisotropy. Samples with a high value are mostly effected by mineral composition (meta-basite)

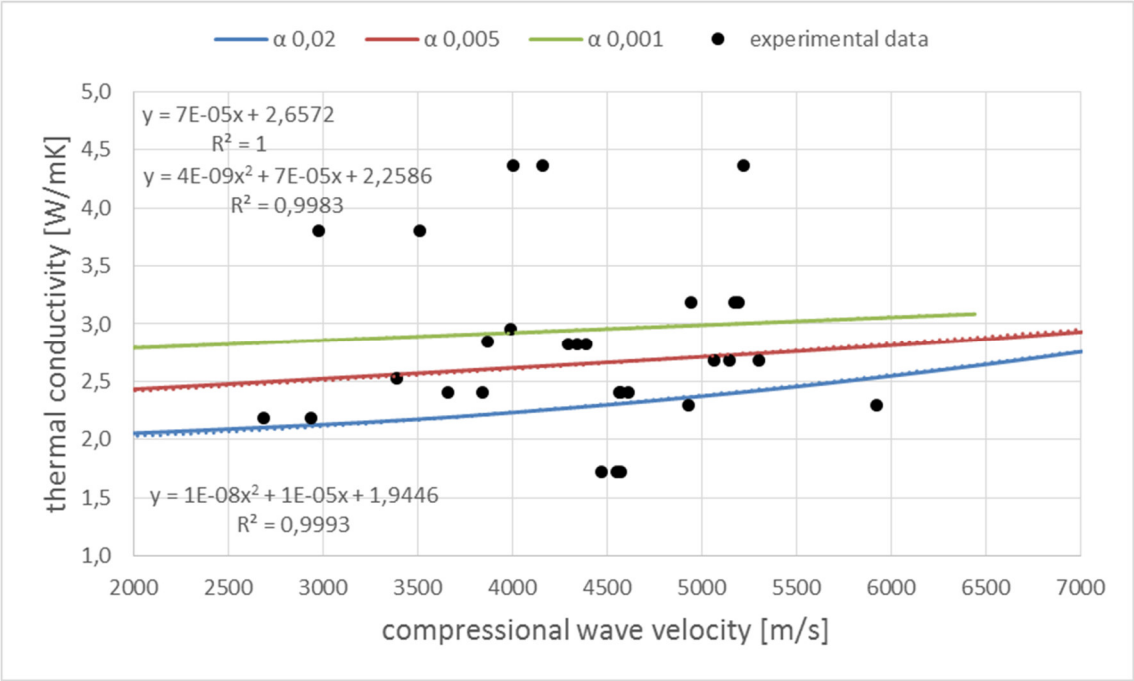

Figure 20: Thermal conductivity vs. compressional wave velocity (basalt 1) (points= experimental data, curves= calculated data for different aspect ratios)

Table 7 presents the resulting regression equations for the lithology.

Rocktype	aspect ratio	Regression equations	R^2
Basalt	0.001	λ=7E-05*v_p + 2.66	1
Basalt	0.005	λ=4E-09*v_p^2 + 7E-05*v_p + 2.26	0.998
Basalt	0.02	λ=1E-08*v_p^2 + 1E-05*v_p + 1.94	0.999

Table 7: Regressions and coefficient of determination from calculated curves for different aspect ratios (basalt 1) (λ in W/mK, v_p in m/s)

6. Application on log data and comparison

The main task of the Master thesis is to develop a model calculation out of experimental laboratory data, which can describe the thermal conductivity from conventional logs. To plot and interpret the log data the program “Interactive Petrophysics” from the company Senergy is used.

6.1. Thermal conductivity calculation out of the Sonic log

In the first case the Sonic log is used to calculate the regressions for the thermal conductivity. Sonic logs are almost always available and the compressional wave velocity shows a strong connection with the thermal conductivity. Figure 21 shows a flow chart of the different steps for the model calculation.

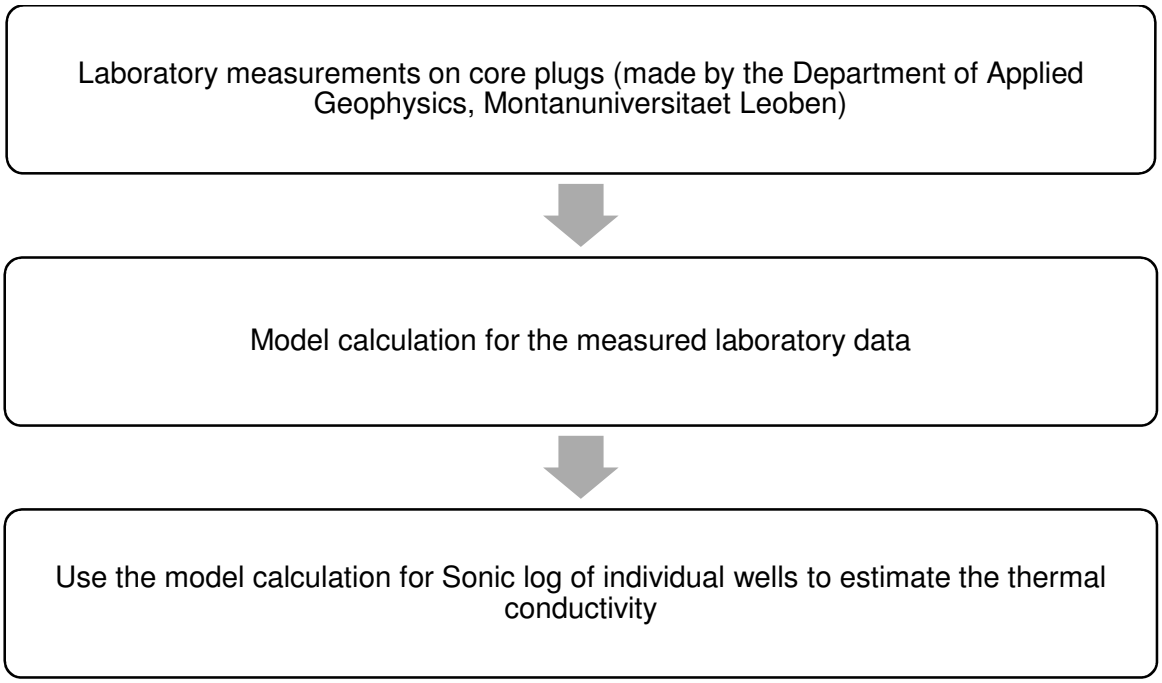

Figure 21: Flow Chart of working plan for model calculation

For model calculation (Chapter 4.) every lithology was considered separately to respect mineral composition and pore shape. This calculations lead to a “thermal conductivity log” out of the Sonic log. The regressions for the model calculation are presented in Chapter 5.

6.1.1. KTB - continental deep drilling project

The KTB is an excellent well for this project, because all needed measurements are available to a depth of 4000 meter. Additionally thermal conductivity data is available from core data. The geographic location is presented in Chapter 2.

The model calculations are applied on the lithologies gneiss and metabasite for different depth intervals. Figure 22 presents the first considered well section of KTB from 1100 to 1900 meter.

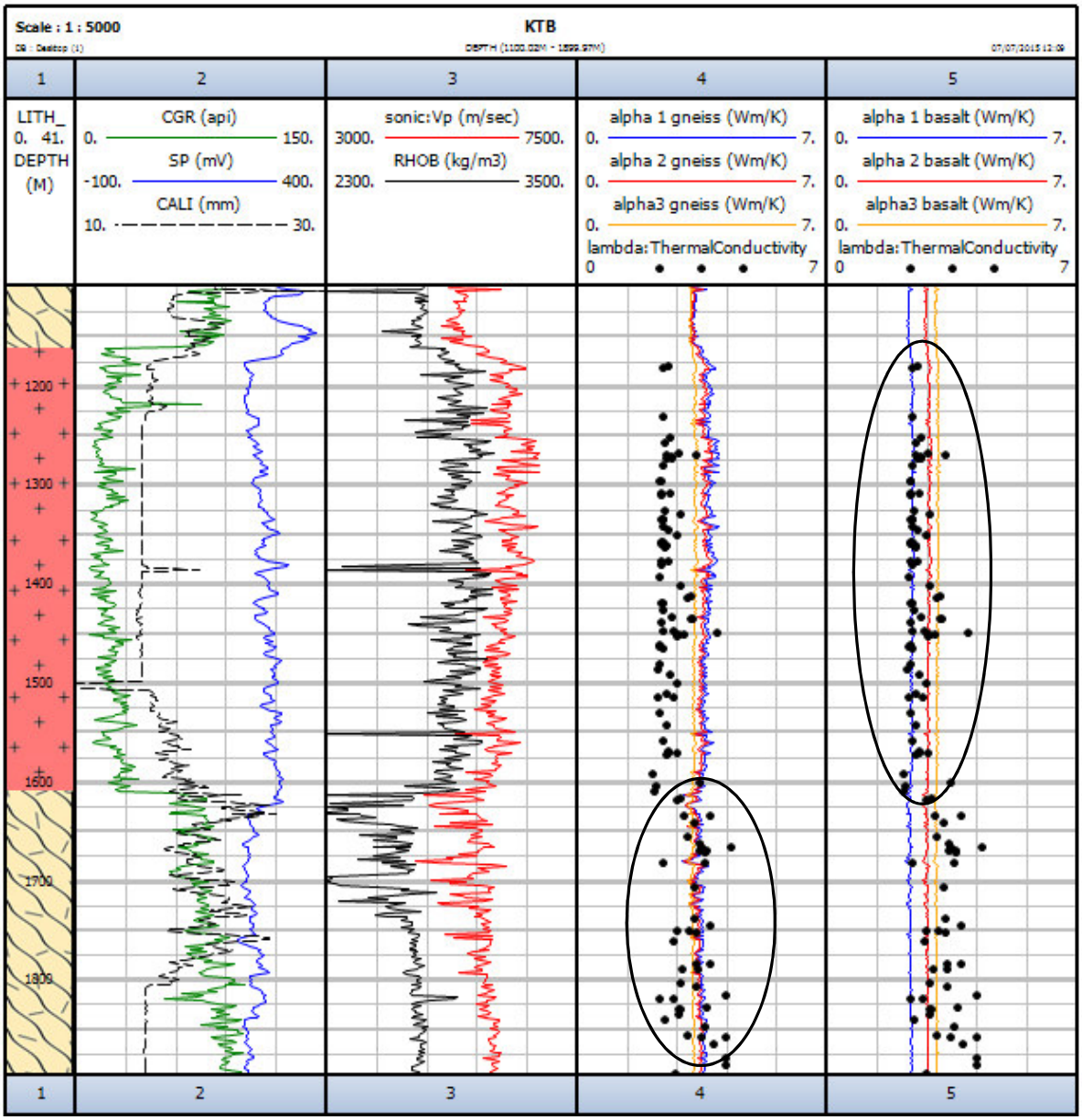

Figure 22: Well KTB (1100 to 1900 meter): trace 1: lithology (cream with lines= gneiss; red with crosses= metabasite); trace 2: corrected-gamma-log, self-potential-log, caliper log; trace 3: Vp calculated from Sonic log and density log; trace 4: lines= calculated thermal conductivity gneiss for different aspect ratios, points= core data; trace 5: lines= calculated thermal conductivity basalt for different aspect ratios, points= core data

Two models (gneiss and basalt) are used to determine the thermal conductivity from the Sonic log. If we compare these models the difference in the calculated “thermal conductivity log” is obvious. Metabasites show lower thermal conductivity and therefore the model for granite/gneiss would lead to too high values. If just the model for basalt is used the sections for gneiss would be underestimated. The thermal conductivity of the core data varies in a broad area because of anisotropy effects. Therefore the three different aspect ratios give a better range for the thermal conductivity. Figure 23 shows log data from 2800 to 3900 meter.

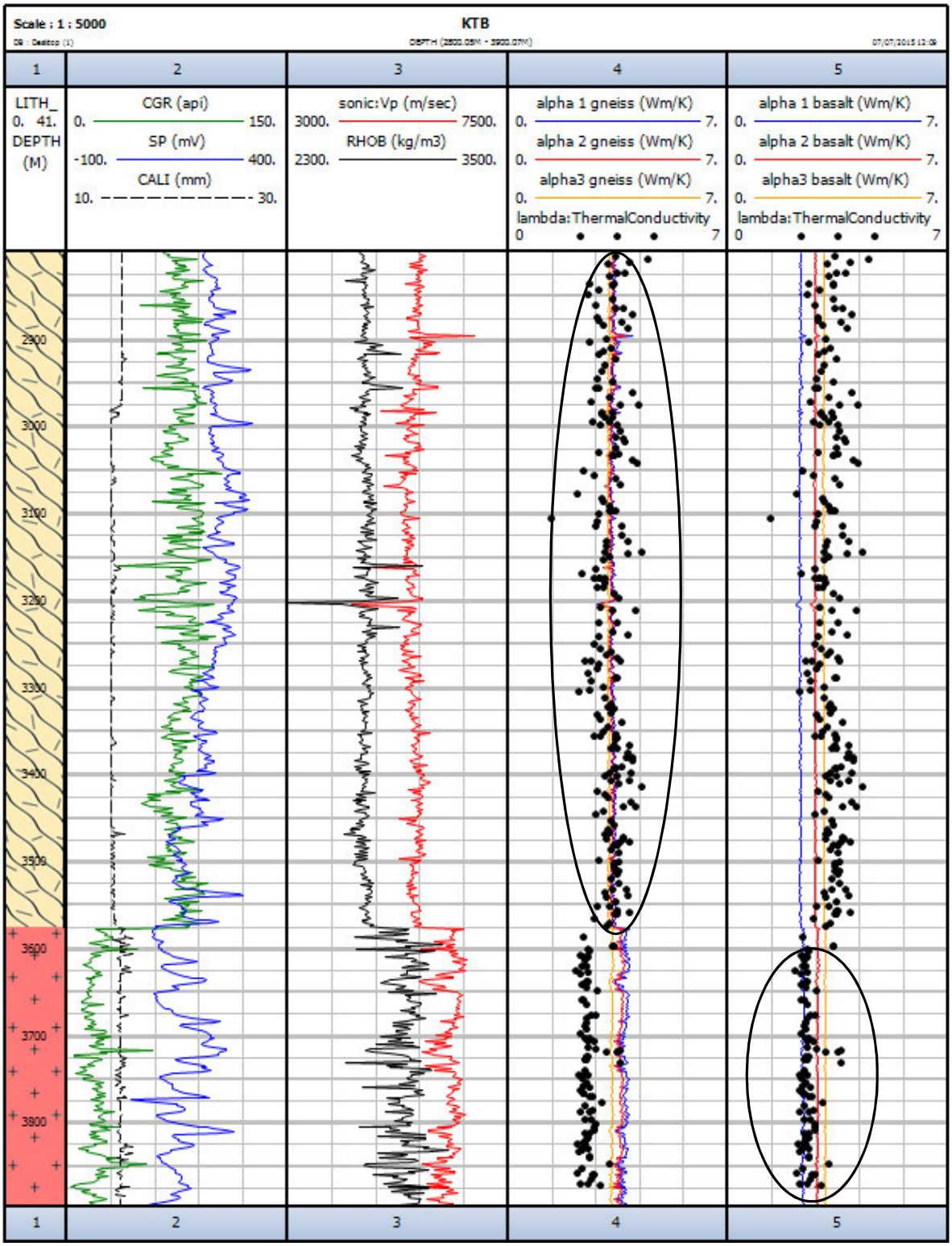

Figure 23: Well KTB (2800 to 3900 meter): trace 1: lithology (cream with lines= gneiss; red with crosses= metabasite); trace 2: corrected-gamma-log, self-potential-log, caliper log; trace 3: vp calculated from Sonic log and density log; trace 4: lines= calculated thermal conductivity gneiss for different aspect ratios, points= core data; trace 5: lines= calculated thermal conductivity basalt for different aspect ratios, points= core data

Again the different lithologies need different models to get a significant correlation of the calculated log with the core data. Therefore the lithology is an important factor for the models.

If the lithology is known (in most wells this is the case, because of cuttings and logs) the right model can be used and gives a good fit with the real data.

The model doesn´t show an influence of depth. The density normally increases with depth and therefore also the velocity of the compressional wave. This effect cannot be observed for the KTB. The reason is maybe a low porosity of the formation rocks.

To test the models for phyllite, sandstone and mica schist more well data would be needed.

6.2. Thermal conductivity estimation out of the Resistivity log

The specific electrical resistivity of a formation is highly affected by the pore space and their filling. Most of the minerals are isolators, therefore the resistivity log cannot distinguish between the lithologies. However the results in Chapter 5 of the laboratory samples show a strong correlation of the formation factor and the thermal conductivity. Therefore the model is tested on the KTB data. For the Resistivity log the LLD (Laterolog Deep) is used. With this log and the resistivity of the mud (Rw) the formation factor (F) is calculated:

$$F = \frac{R_0}{R_w}$$

In the next step, the regression lines for each lithology (from the laboratory data, also see Figure 8) are calculated and applied on the log data. In Figure 24 the results of the estimated thermal conductivity in the area of 1200 to 1900 meter for the lithology gneiss and basalt is plotted. The regression lines fit the real data not very good and vary over a broad range. The reason is a bad correlation of the regression lines with the calculated lines in Excel (R^2= 0.80-0.85).

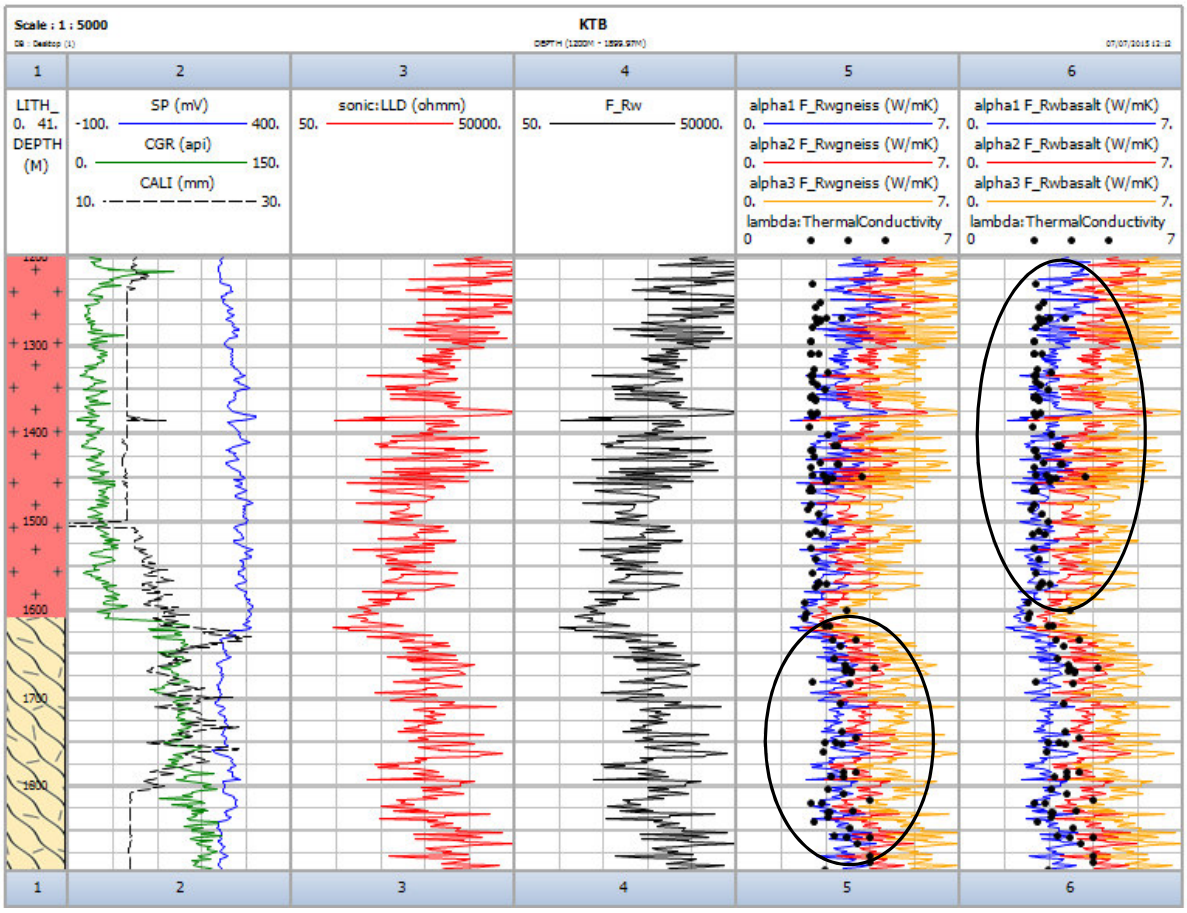

Figure 24: Well KTB (1200 to 1900 meter): trace 1: lithology (cream with lines= gneiss; red with crosses= metabasite); trace 2: corrected-gamma-log, self-potential-log, caliper log; trace 3: Laterolog Deep; 4: calculated formation factor 5: lines= calculated thermal conductivity gneiss for different aspect ratios, points= core data; trace 6: lines= calculated thermal conductivity basalt for different aspect ratios, points= core data

In order to get a useful result a better derivation of the equations is needed. Gegenhuber (2013) describes the correlation of the porosity and the formation factor with the equation:

$$\Phi = \frac{1}{\sqrt{F}}$$

Therefore the values for the formation factor are transformed and a good fit of the regression curves with the core data is possible. Figure 25 shows the results of the modified formation factor ($1/\sqrt{F}$). Compared to the result of the Sonic log estimation, also here the difference of the different lithologies can be recognized. The calculated data for basalt is a little too high and this result confirm the observations in the laboratory data for the model design.

The values for granite/gneiss model are higher and therefore would lead to an overestimation in the area of basalt.

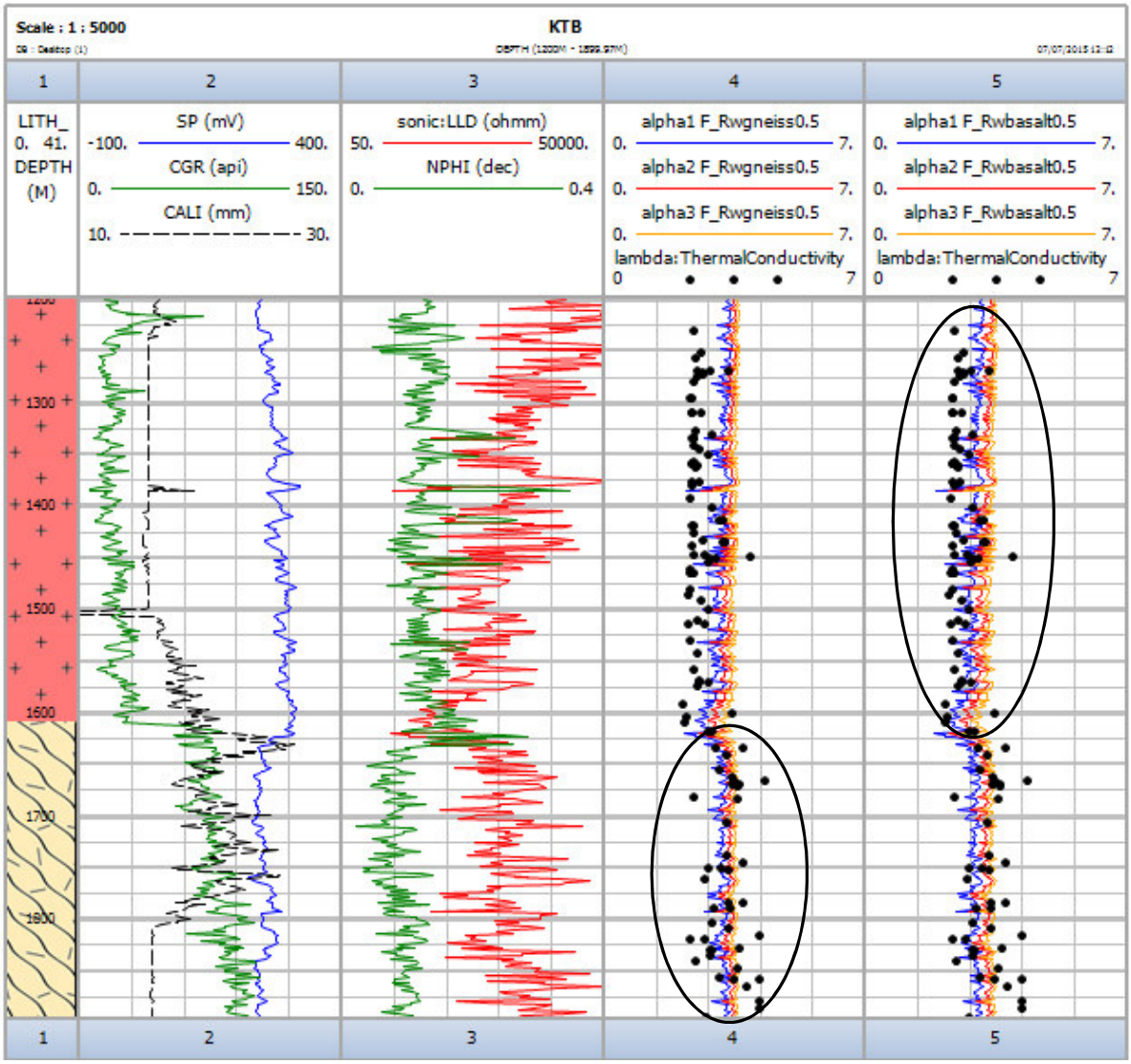

Figure 25: Well KTB (1200 to 1900 meter): trace 1: lithology (cream with lines= gneiss; red with crosses= metabasite); trace 2: corrected-gamma-log, self-potential-log, caliper log; trace 3: red= Laterolog deep, green= Neutron Log; trace 4: lines= calculated thermal conductivity gneiss for different aspect ratios, points= core data; trace 5: lines= calculated thermal conductivity basalt for different aspect ratios, points= core data

Table 8 presents the used regression equations for the modified formation factor.

Rocktype	aspect ratio	Regression equations	R^2
Granite/Gneiss	0.003	$\lambda = -34.406x^2 - 8.1795x + 3.6431$	0.999
Granite/Gneiss	0.01	$\lambda = -11.174x^2 - 13.915x + 3.5907$	0.999
Granite/Gneiss	0.02	$\lambda = 15.174x^2 - 19.627x + 3.4746$	0.999
Basalt	0.001	$\lambda = -26.384x^2 - 11.889x + 3.559$	0.998
Basalt	0.005	$\lambda = -2.803x^2 - 17.92x + 3.4954$	0.998
Basalt	0.02	$\lambda = 22.654x^2 - 20.956x + 3.238$	1

Table 8: Regressions and coefficient of determination from calculated modified formation factor curves for different aspect ratios (basalt and granite/gneiss) (λ in W/mK)

Figure 26 shows the lower section of the well (2800m to 3900m) where the same trend can be observed.

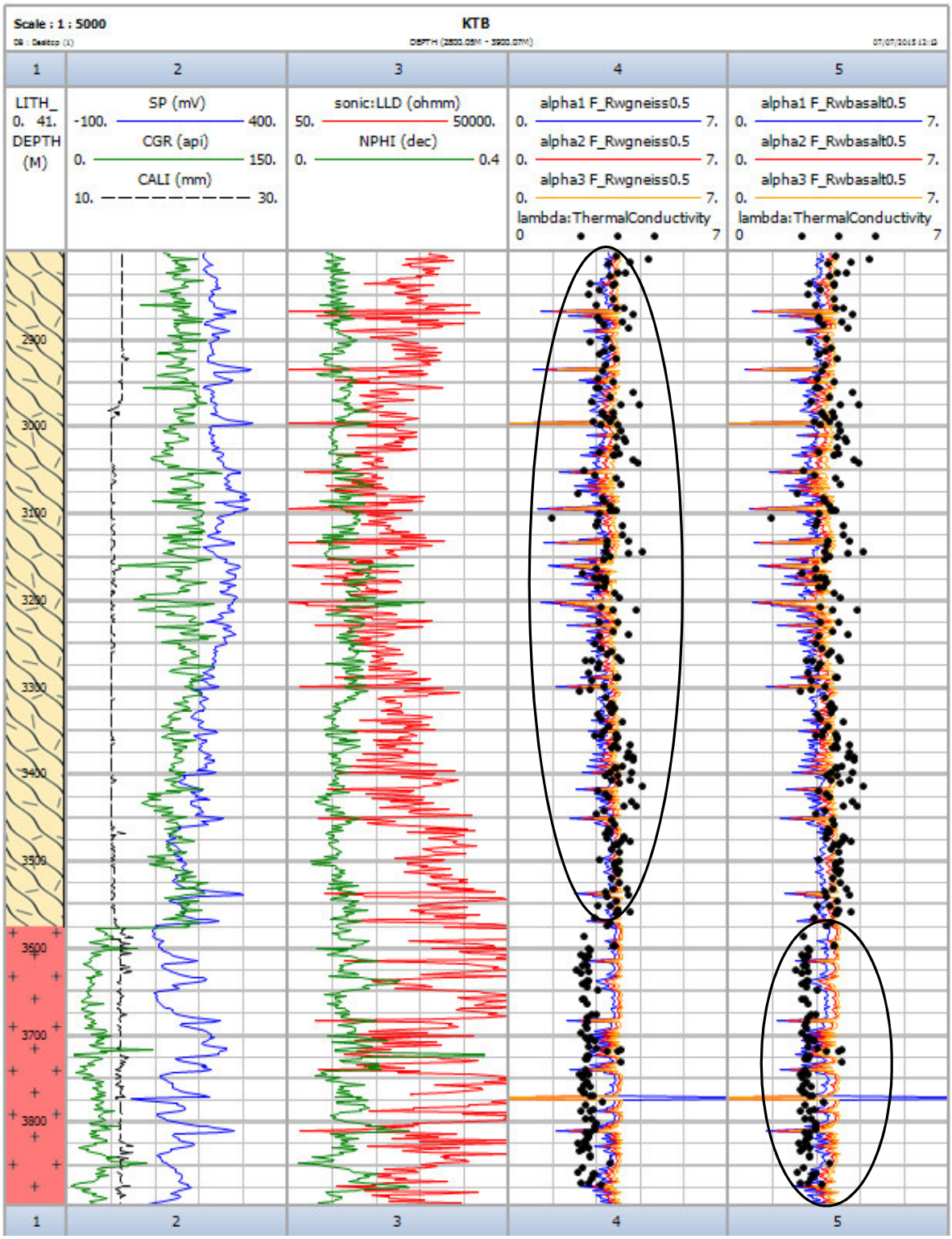

Figure 26: Well KTB (2800 to 3900 meter): trace 1: lithology (cream with lines= gneiss; red with crosses= metabasite); trace 2: corrected-gamma-log, self-potential-log, caliper log; trace 3: red= Laterolog deep, green= Neutron Log; trace 4: lines= calculated thermal conductivity gneiss for different aspect ratios, points= core data; trace 5: lines= calculated thermal conductivity basalt for different aspect ratios, points= core data

6.3. Comparison model results with real data

For interpretation of the calculated models again the KTB data is used (25 to 4000 meter) and the following cross plots are sorted for the two lithologies granite/gneiss and basalt. Also the aspect ratio is considered (alpha 1 and alpha 3). Presented cross plots are:

- Thermal conductivity versus Sonic calculated thermal conductivity
- Thermal conductivity versus Resistivity calculated thermal conductivity
- Sonic calculated versus Resistivity calculated thermal conductivity

Figure 27 shows the real data compared with the calculated data from the Sonic log for the lithology granite/gneiss. The values for alpha 3 range in a smaller area as for alpha 1, because flatter pores are assumed.

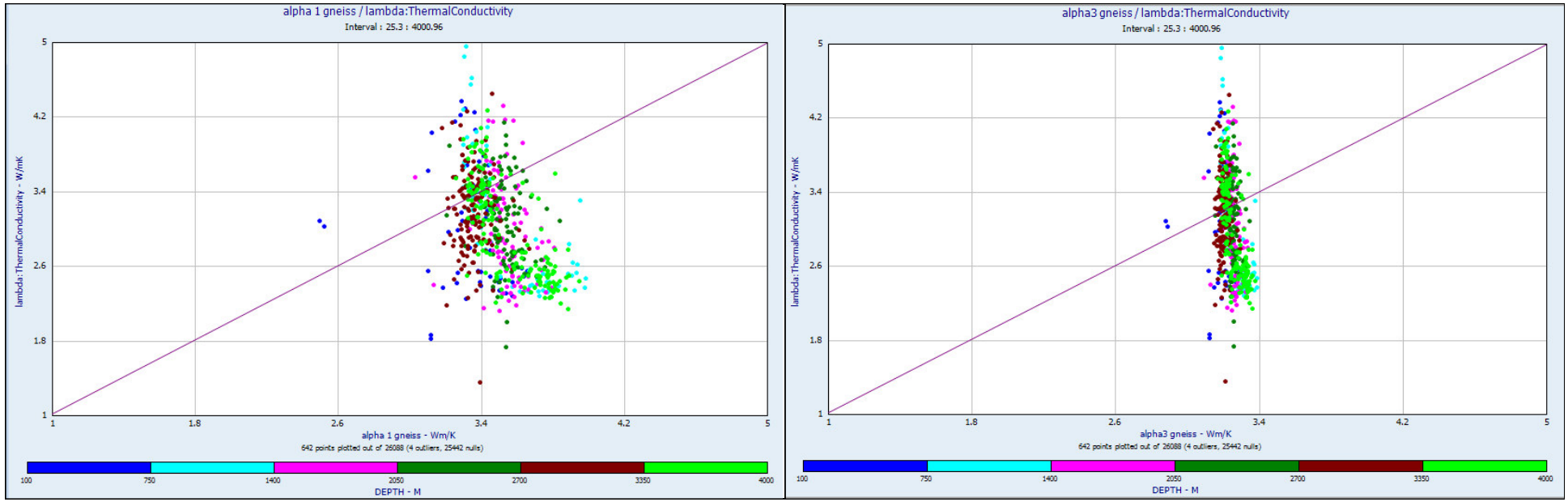

Figure 27: Comparison real data with Sonic calculated thermal conductivity (granite/gneiss); y-axis= thermal conductivity real data; x-axis= thermal conductivity estimated from Sonic log; colors mark the depth zones

Colors mark the different depth zones and a depth influence for the model cannot be observed.

Figure 28 compares the measured thermal conductivity with the thermal conductivity calculated from the Resistivity log for the lithology granite/gneiss. Compared with the Sonic estimated values here the data varies over a larger range. Again there is no indication of a depth dependence of the applied model.

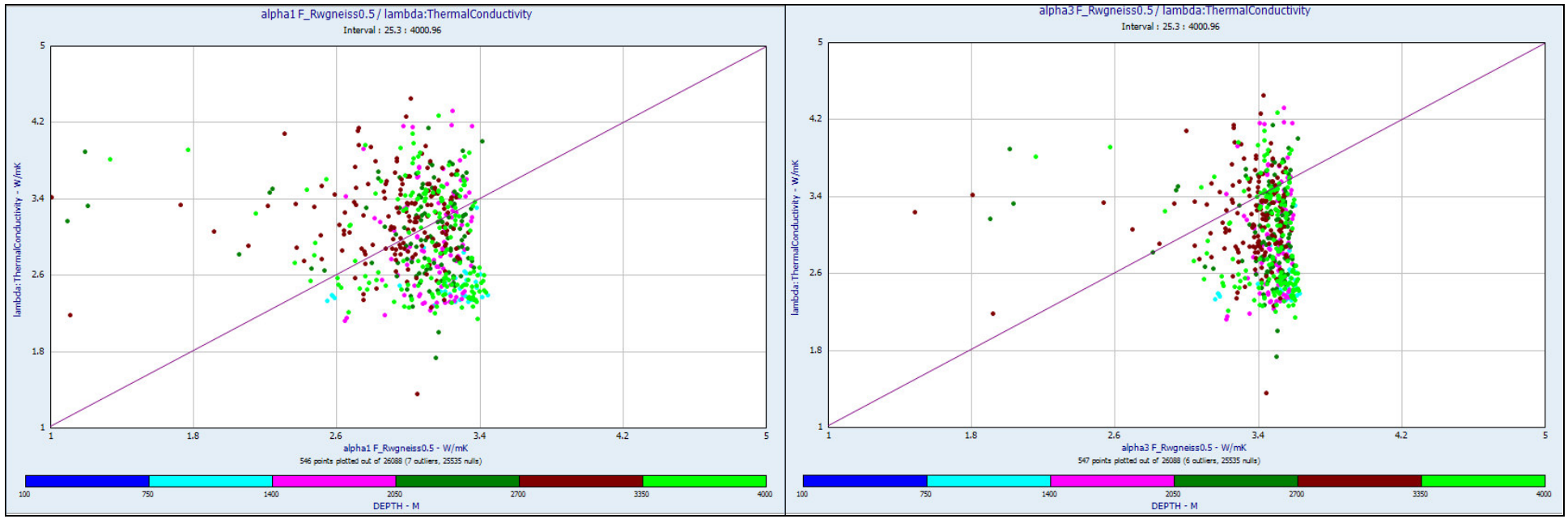

Figure 28: Comparison real data with resistivity calculated thermal conductivity (granite/gneiss); y-axis= thermal conductivity real data; x-axis= thermal conductivity estimated from Resistivity log; colors mark the depth zones

In Figure 27 and Figure 28 a few outliers occur, which can be neglected. Anisotropy and mineralogy have an important influence on the thermal conductivity and lead to a broad range of the measured data.

Figure 29 shows the real data compared with the calculated data from the Sonic log for the lithology basalt.

The difference between alpha 1 and alpha 3 is clearly visible. Values for alpha 3 again presume flatter pores and the velocity increases. This effect is not visible for gneiss. The data is colored for different depth intervals and again a depth influence on the model cannot be observed.

The Sonic calculated data ranges in a small area for the lithology basalt. The reason why the values for the calculated thermal conductivity vary not so wide is the spacing of the measurement. Real data is measured on plugs, therefore has a spacing of just a few centimeters and the data vary over a large area. The Spacing of the Resistivity- and the Sonic log is in the area of decimeter and therefore the resulting values are not so variable and smoothed.

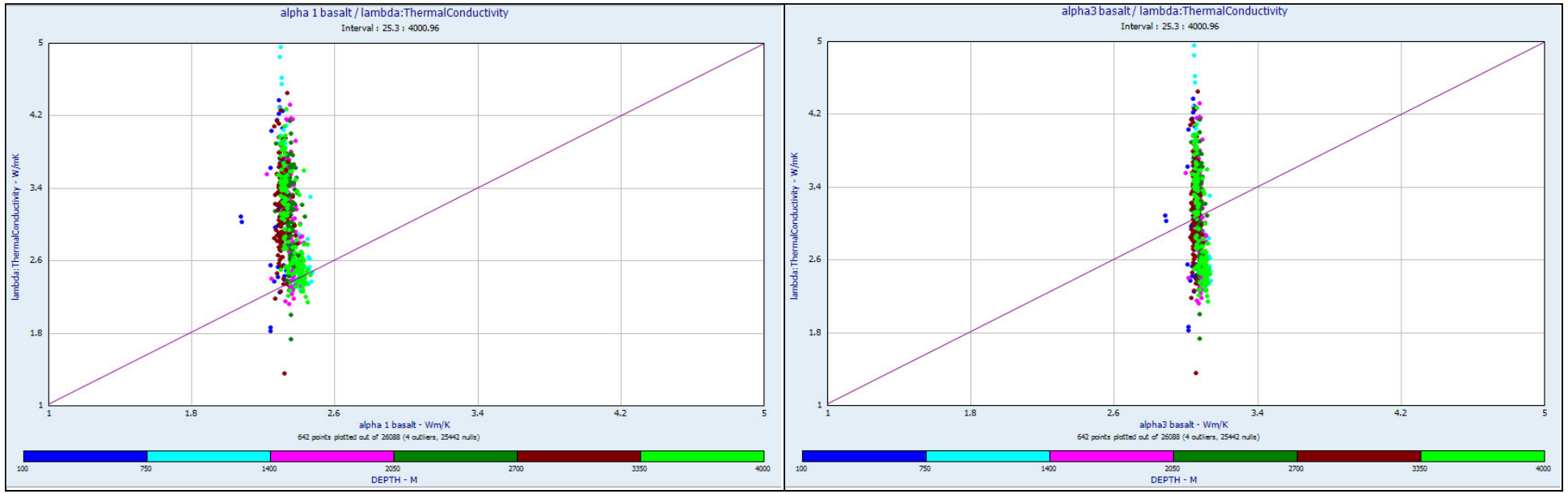

Figure 29: Comparison real data with Sonic calculated thermal conductivity (basalt); y-axis= thermal conductivity real data; x-axis= thermal conductivity estimated from Sonic log; colors mark the depth zones

Figure 30 compares the measured thermal conductivity with the thermal conductivity calculated from the Resistivity log for the lithology basalt.

Here the basalt can be compared with the granite/gneiss lithology very well. Again no depth influence is visible and the measured data spreads over a large range.

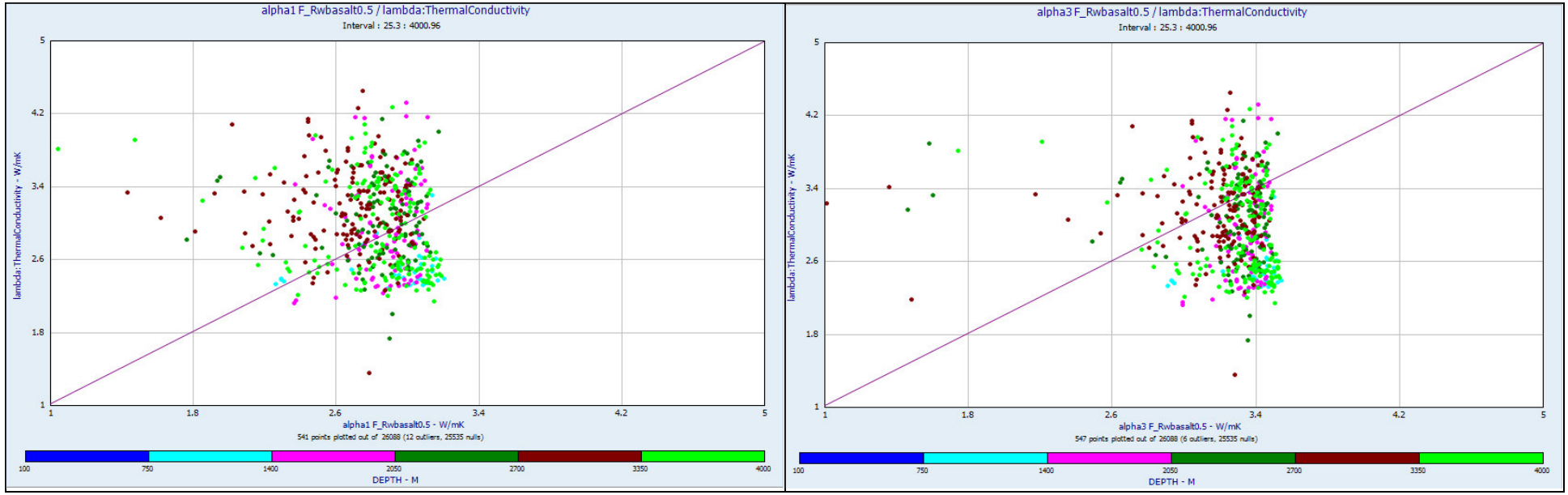

Figure 30: Comparison real data with resistivity calculated thermal conductivity (basalt); y-axis= thermal conductivity real data; x-axis= thermal conductivity estimated from Resistivity log; colors mark the depth zones

Figure 31 shows the cross plot between the Sonic calculated thermal conductivity (x-axis) and the resistivity calculated thermal conductivity (y-axis) for the lithology granite/gneiss.

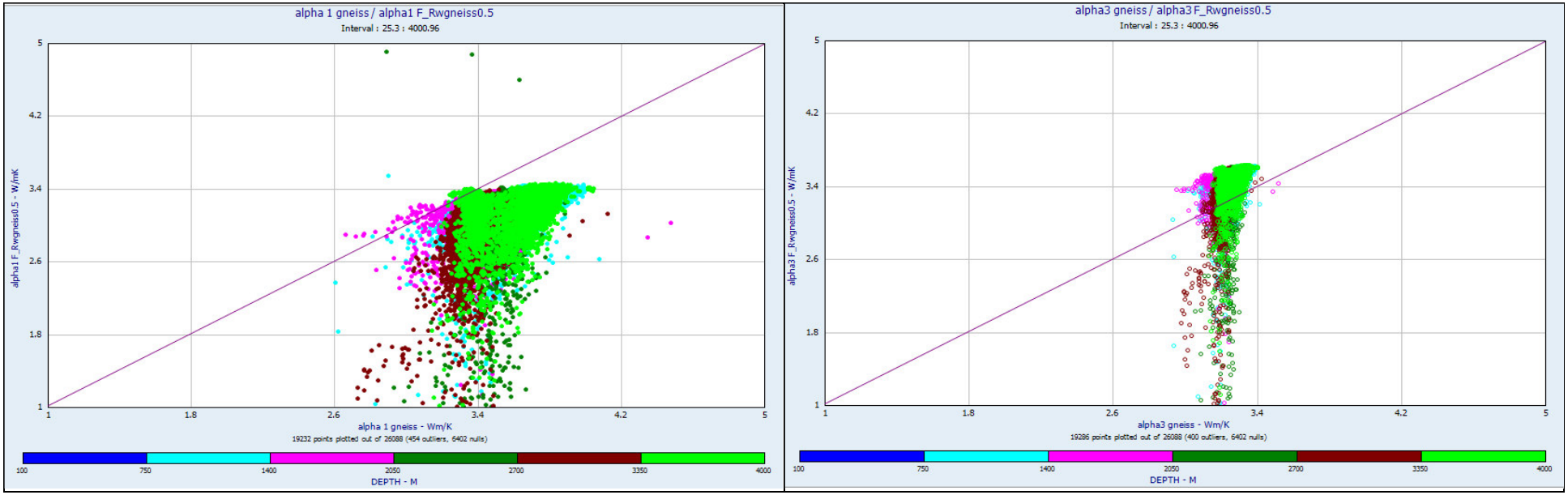

Figure 31: Cross plots gneiss; y-axis= thermal conductivity estimated from Resistivity log; x-axis= thermal conductivity estimated from Sonic log (left side alpha 1, right side alpha 3); colors mark the depth zones

The graph clearly shows higher values for thermal conductivity calculated from the Sonic log. The data is colored for different depth zones and an increase in thermal conductivity with increasing depth cannot be recognized. In this case the high amount of data points overlie each other, which can lead to a wrong interpretation very easily. The anisotropy effect and mineralogy influence lead to a wide spread of the data.

The lithology basalt (Figure 32) varies in a wide range within the resistivity calculated thermal conductivity. The Sonic log based model ranges in a smaller area. Again no depth influence can be observed.

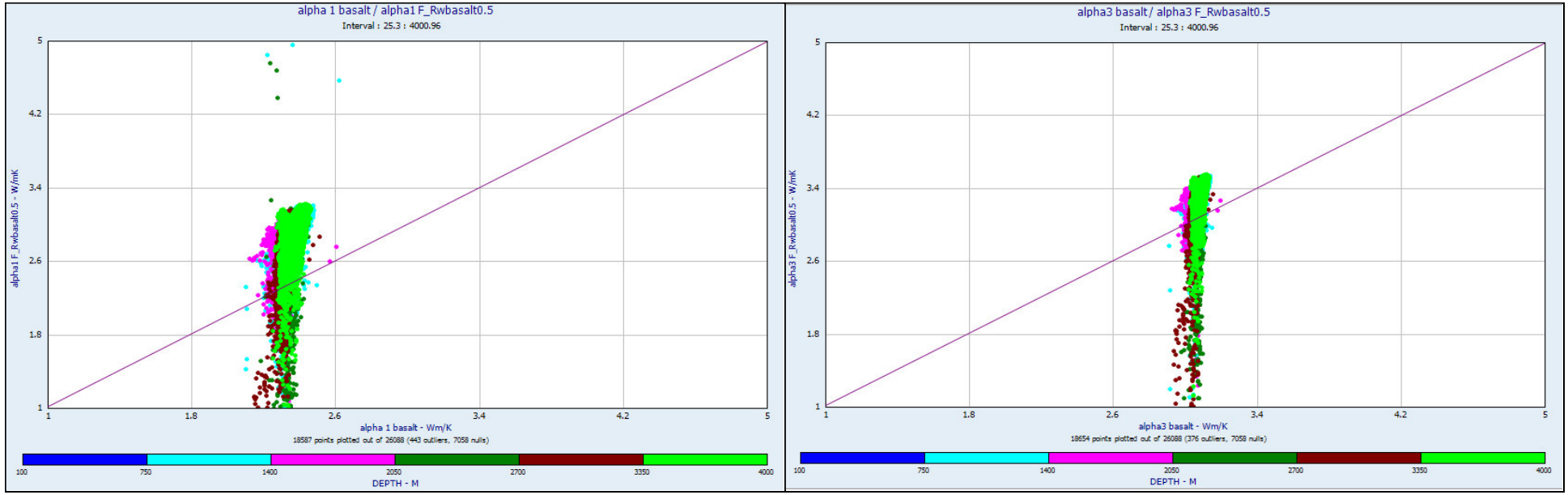

Figure 32: Cross plot basalt; y-axis= thermal conductivity estimated from Resistivity log; x-axis= thermal conductivity estimated from Sonic log (left side alpha 1, right side alpha 3); colors mark the depth zones

In summary the cross plots show:

- A strong influence of the rock type
- A broad scatter of the measured “real” data
- Great influence of anisotropy
- Differences in pore shape (aspect ratio) affect the model calculation significant most of the time

6.4. Histograms

To illustrate the correlation of measured and calculated data the following histograms are shown for the lithologies a) gneiss (Well KTB from 2800 to 3500 meter depth) and b) basalt (Well KTB from 3600 to 3900 meter depth).

a) Gneiss

Figure 33 shows the measured “real” data of thermal conductivity.

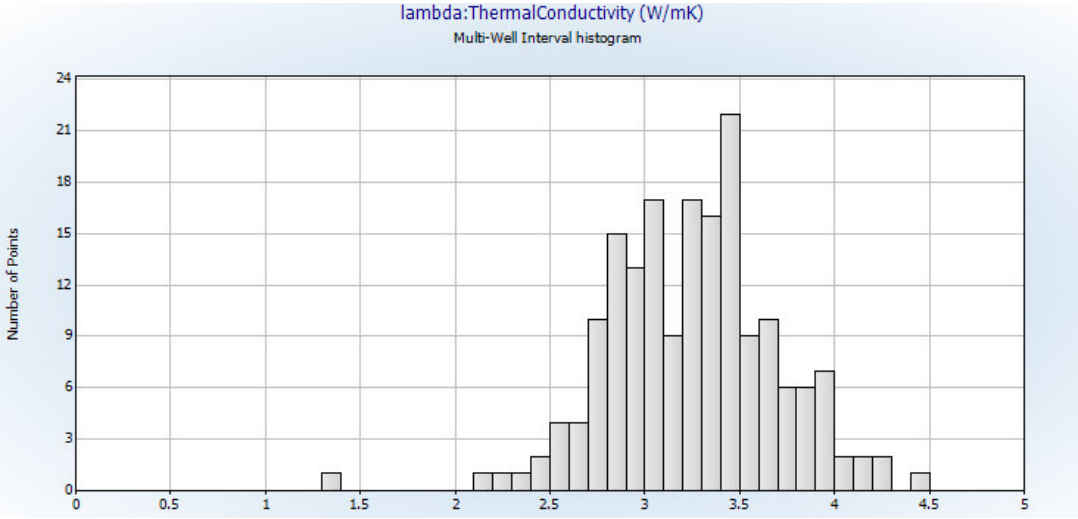

Figure 33: Measured thermal conductivity (Well KTB from 2800 to 3500 meter) (gneiss); x-axis= thermal conductivity (W/mK)

Figure 34 shows the histogram of the Sonic calculated thermal conductivity.

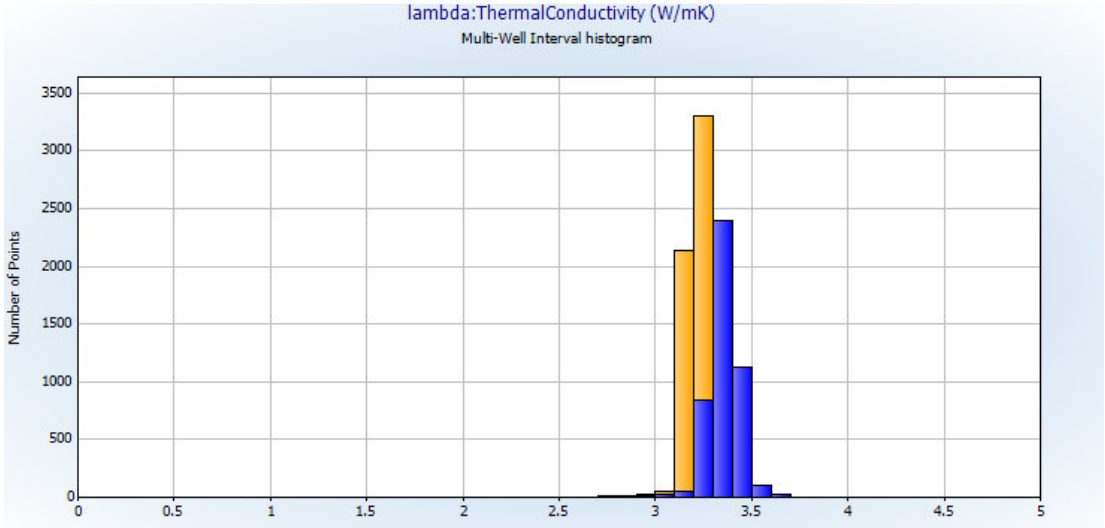

Figure 34: Sonic calculated thermal conductivity (Well KTB from 2800 to 3500 meter) (gneiss); x-axis= thermal conductivity (W/mK); blue= alpha 1, orange= alpha 3

Figure 35 shows the histogram of the resistivity calculated thermal conductivity.

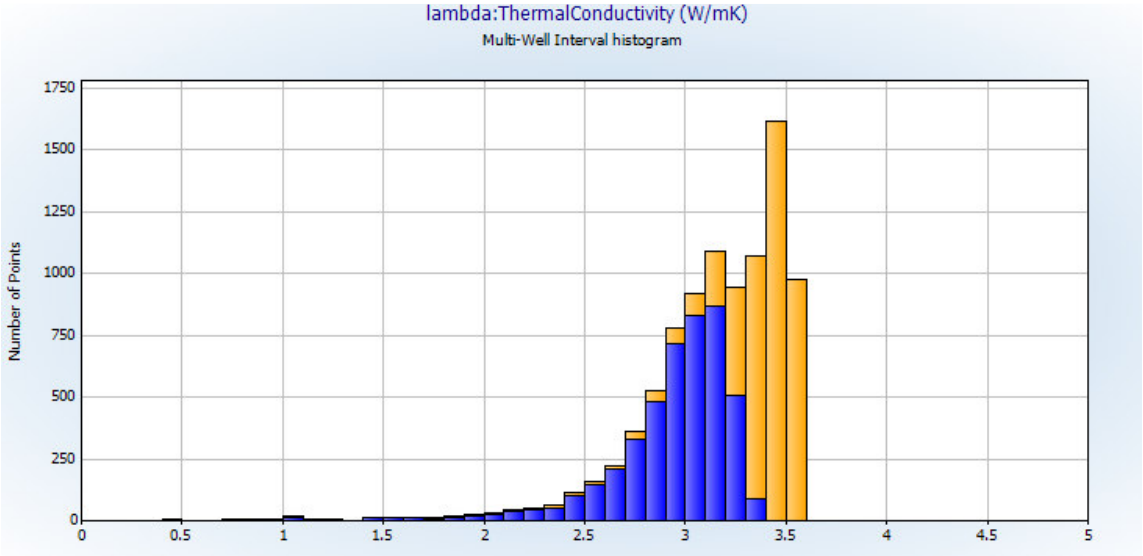

Figure 35: Resistivity calculated thermal conductivity (Well KTB from 2800 to 3500 meter) (gneiss); x-axis= thermal conductivity (W/mK); blue= alpha 1, orange= alpha 3

b) Basalt

Figure 36 shows the histogram of the measured data of thermal conductivity for the lithology basalt.

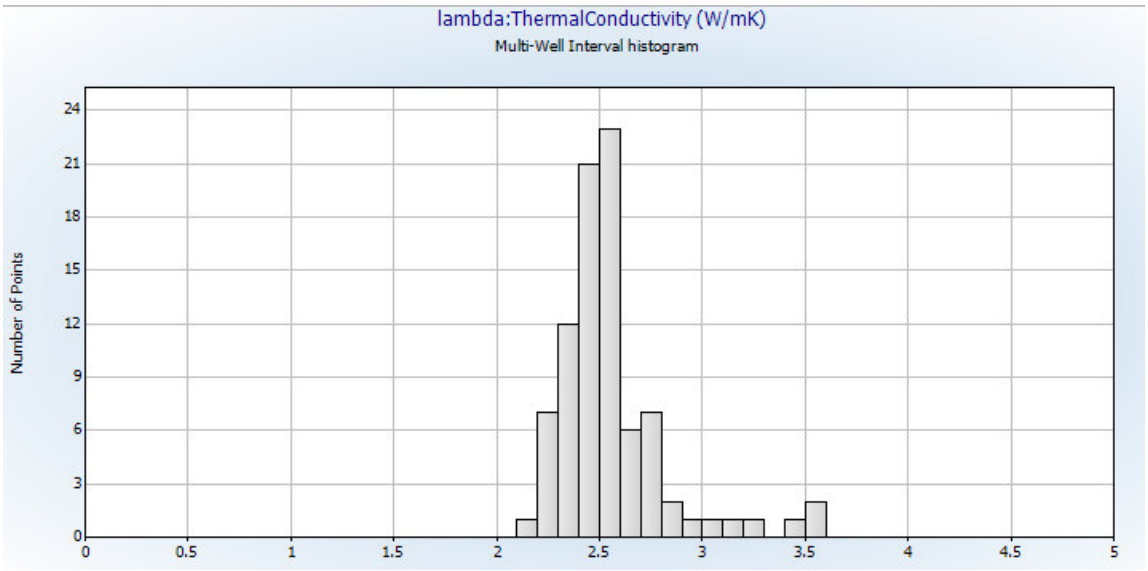

Figure 36: Measured thermal conductivity (Well KTB from 3600 to 3900 meter) (basalt); x-axis= thermal conductivity (W/mK)

Figure 37 shows the histogram of the Sonic calculated thermal conductivity.

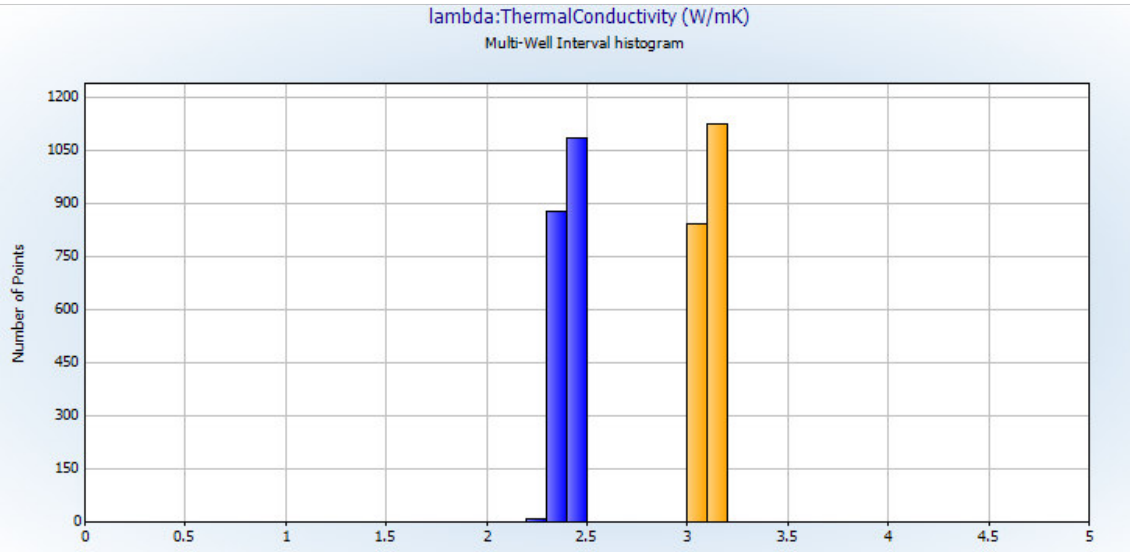

Figure 37: Sonic calculated thermal conductivity (Well KTB from 3600 to 3900 meter) (basalt); x-axis= thermal conductivity (W/mK); blue= alpha 1, orange= alpha 3

Figure 38 shows the histogram of the resistivity calculated thermal conductivity.

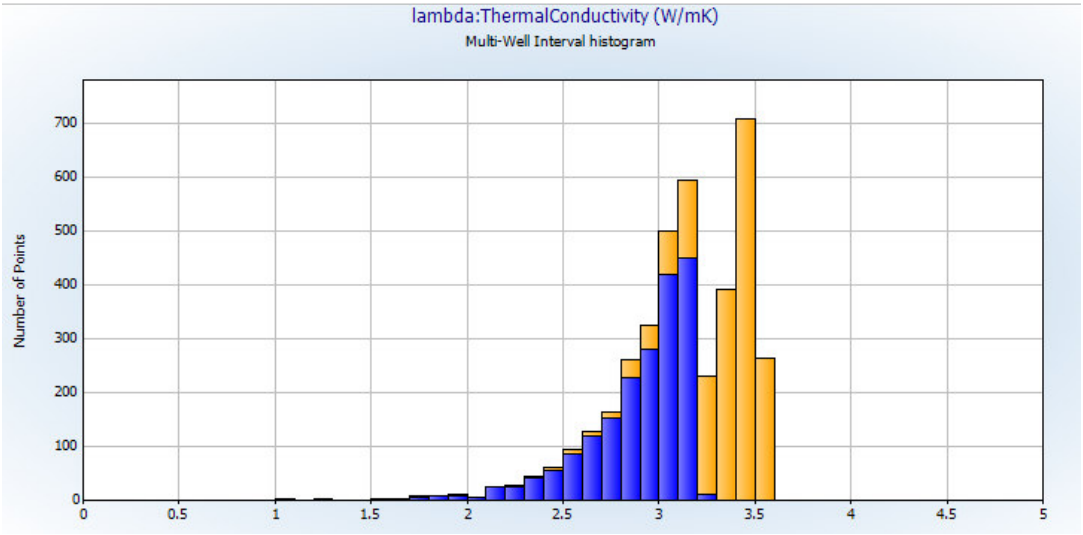

Figure 38: Resistivity calculated thermal conductivity (Well KTB from 3600 to 3900 meter) (basalt); x-axis= thermal conductivity (W/mK); blue= alpha 1, orange= alpha 3

The histograms show that the calculated data and the measured data correlate well. Only the values of the resistivity calculated thermal conductivity for the lithology basalt are too high again.

6.5. Multiple Linear Regression

The relationships between several independent variables can be analyzed with the statistical technique of the Multiple Regression. Gasior & Przelaskowska (2014) used empirical models based on the relationship between thermal conductivity and other petrophysical parameters on well log data from Meso-Paleozoic rocks from Tarnow-Debica. They distinguished between siliciclastic and carbonate rocks and a determination coefficient at minimum > 0.74 indicates the correctness of their models (Gasior & Przelaskowska 2014).

The program Interactive Petrophysics allows the user to predict a result curve from different input logs. The curve to predict is defined and this data is used to create the model. With the different input logs the result curve will be calculated and the percentage used of each log is given. For this regression the curve to predict is the thermal conductivity. The input curves are the corrected gamma ray (CGR), the Laterolog deep (LLD), the inverse velocity of the compression wave (DTCO) and the velocity of the p-wave (Vp). The result is shown in Figure 40.

In order of the high amount of samples and the effect of anisotropy, mineralogy and pore space the thermal conductivity values of the samples vary in a wide range. Figure 39 shows the correlation of thermal conductivity of the KTB data with the Multiple Regression data. Also with this application a depth influence cannot be observed.

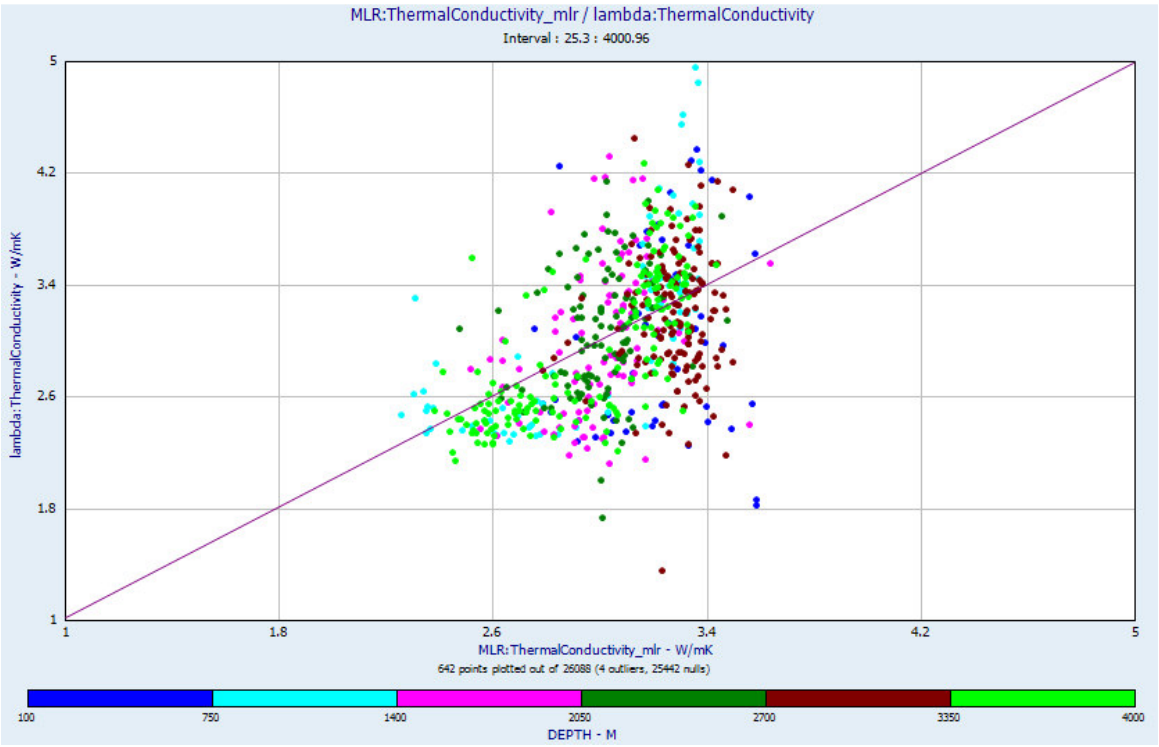

Figure 39: Cross plot Muliple Linear Regression; Y-axis= thermal conductivity real data; X-axis= thermal conductivity calculated with Multiple Linear Regression; colors mark the depth zones

Table 9 shows the used regression formula.

λ = f (Vp, CGR, DTCO, LLD)
λ = 19.6625 - 1.7996E-03*Vp + 1.9081E-06*LLD - 3.5616E-02*DTCO + 3.8869E-04*CGR

Table 9: Multiple Linear Regression Formular

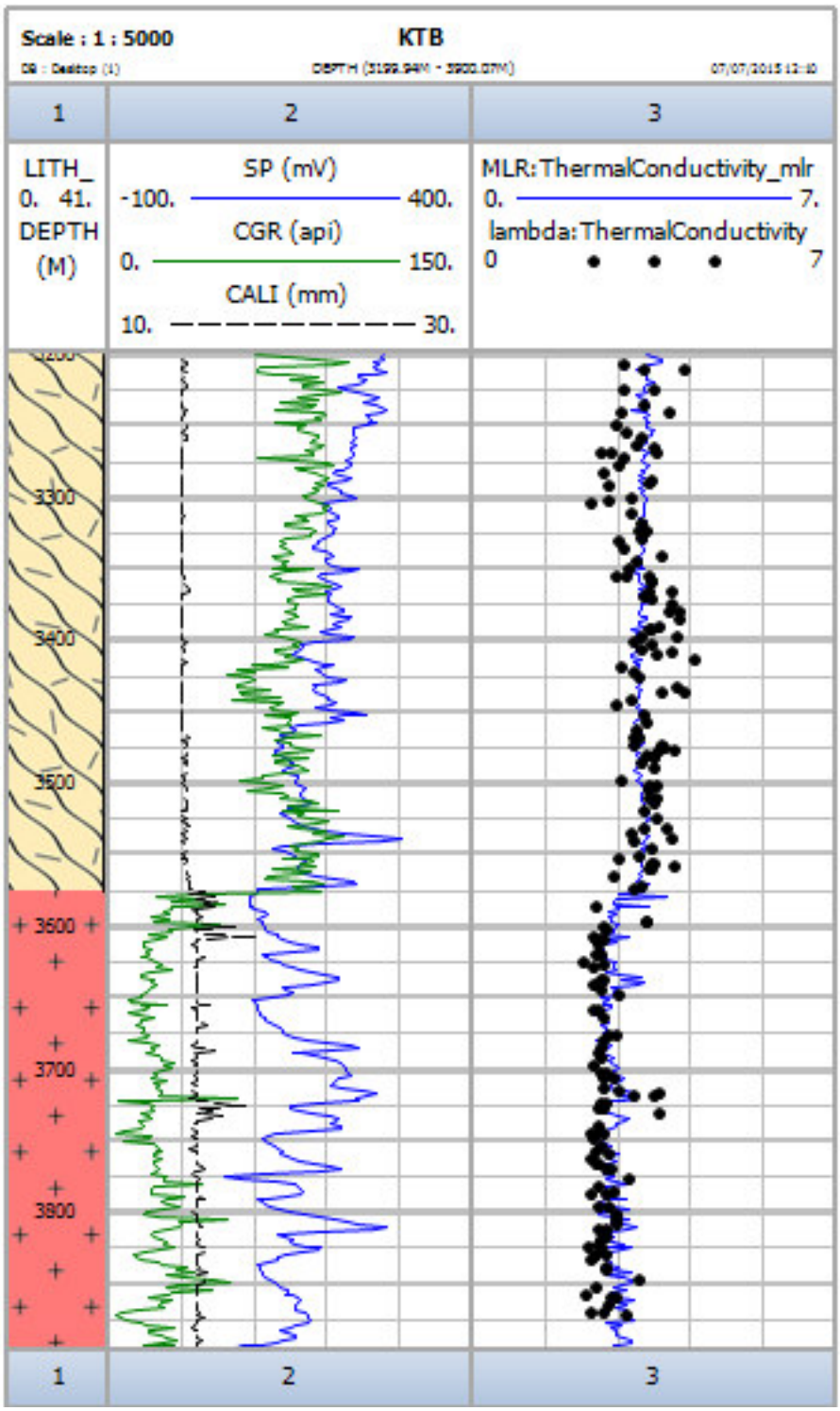

Figure 40: Multiple Linear Regression (Well KTB 3200-3900 meter): trace 1: lithology (cream with lines= gneiss; red with crosses= metabasite); trace 2: corrected-gamma-log, self-potential-log, caliper log; trace 3: line= calculated multiple linear regression, points= core data

6.6. Geometric-mean model

Lichtenecker (1924) introduced the geometric-mean model and Fuchs (2013) applied this model to calculate the matrix- and the bulk thermal conductivity:

$$\lambda_m = \sum_{i=1}^{n} \lambda_i{}^{V_i}$$

λ_m… matrix thermal conductivity [W/mK]

λ_i… thermal conductivity each component [W/mK]

V_i… volume fraction each component [ ]

$$\lambda_b = \lambda_m^{1-\Phi} * \lambda_p^{\Phi}$$

λ_b… bulk thermal conductivity [W/mK]

λ_p… thermal conductivity pore fluid [W/mK]

Φ… porosity [ ]

For this model the porosity is predicted from the Neutron log. The thermal conductivity values for the used minerals are literature values (listed in the appendix). The KTB provides data from XRD and therefore the Volume fraction of the main minerals are known. Used minerals are quartz, potassium feldspar, biotite, white mica, amphibolite, chlorite, garnet and plagioclase. Figure 41 and Figure 42 show the results of the applied geometric-mean model.

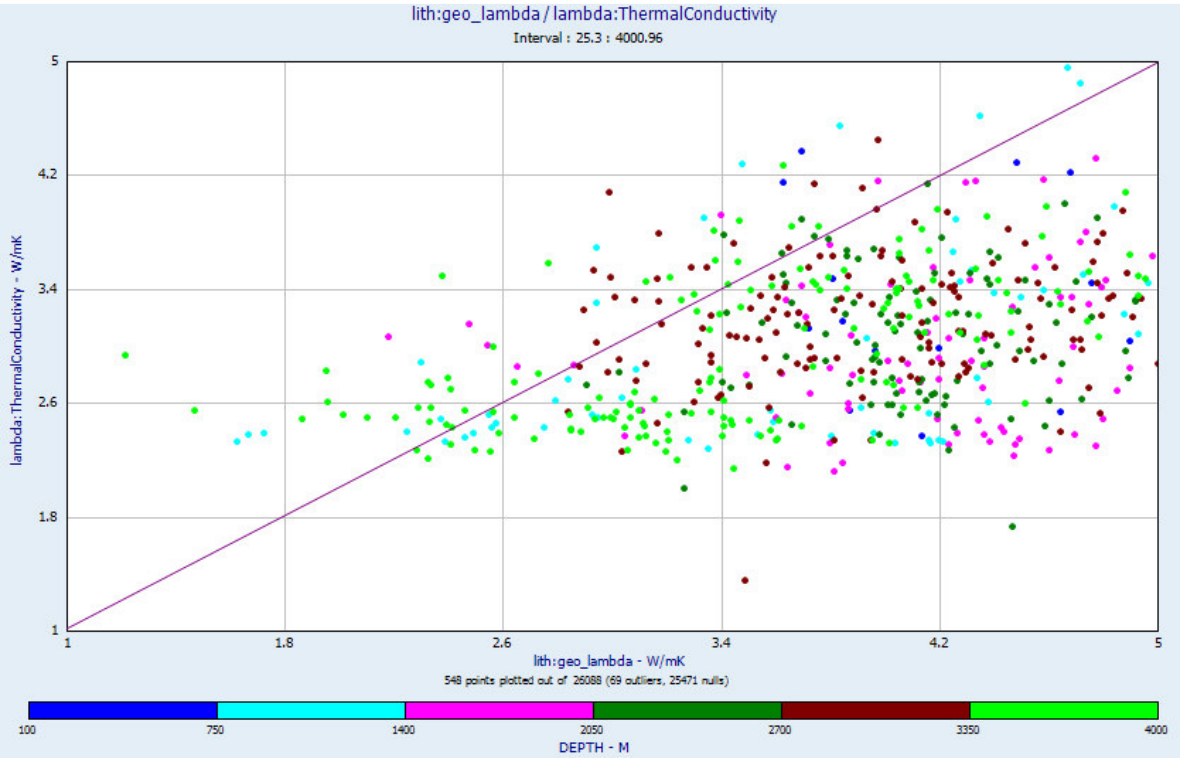

Figure 41: Cross plot geometric-mean model; Y-axis= thermal conductivity real data; X-axis= thermal conductivity calculated with Geometric-mean model; colors mark the depth zones

The cross plot shows a wide spread of the data and a clear trend is not visible.

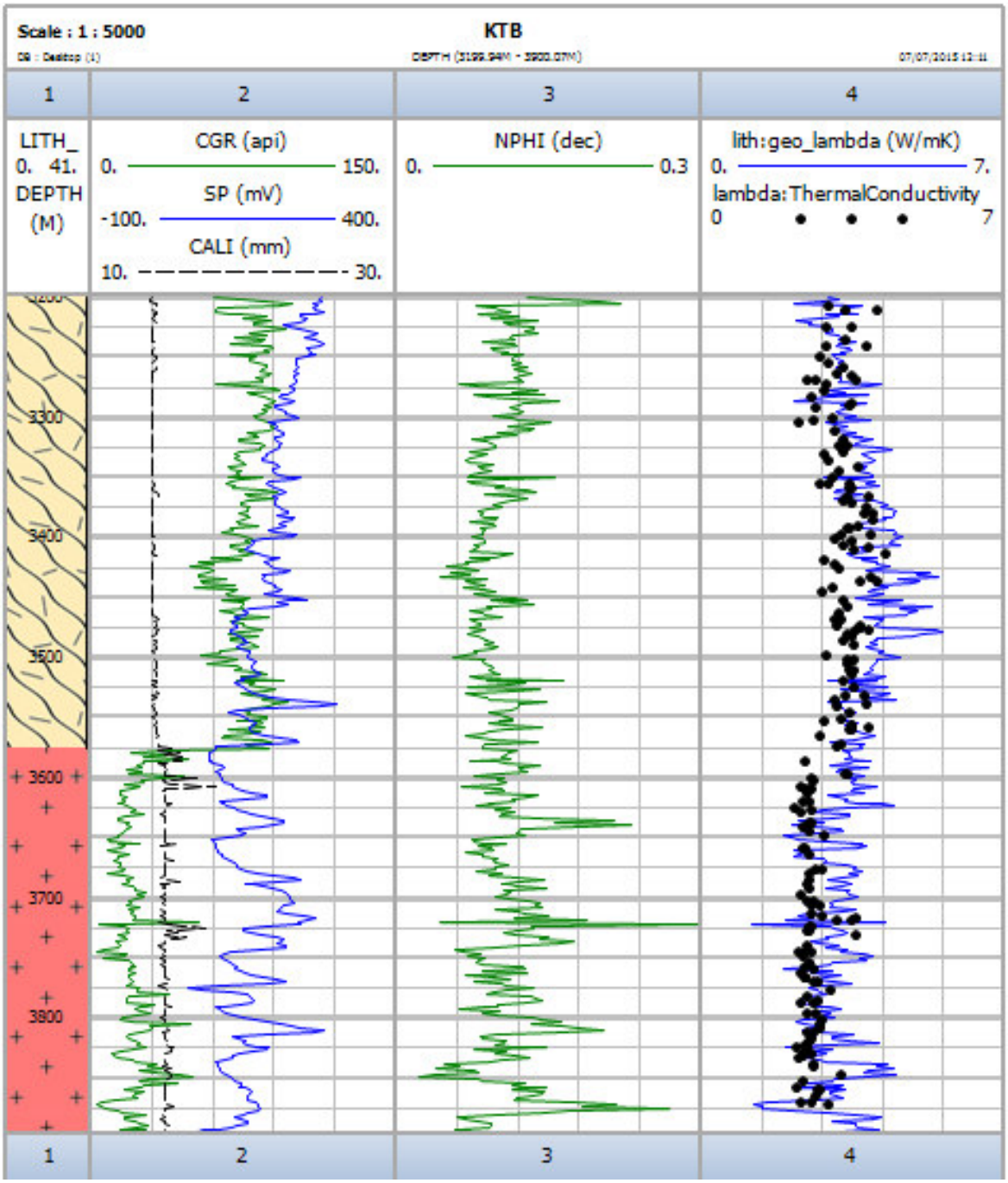

Figure 42: Geometric-mean model (Well KTB 3200-3900 meter): trace 1: lithology (cream with lines= gneiss; red with crosses= metabasite); trace 2: corrected-gamma-log, self-potential-log, caliper log; trace 3: Neutron log; trace 4: line= geometric mean regression, points= core data

The Neutron log indicates a mean porosity between 4 % and 18 %. The model curve follows the trend of the lithology change, but the calculated values are often too high. Again the anisotropy effects the thermal conductivity. The curve varies over a broad range in a small area, because of the turbulent Neutron log.

6.7. Comparison of applied models

In Figure 43 all applied models are shown and can be compared.

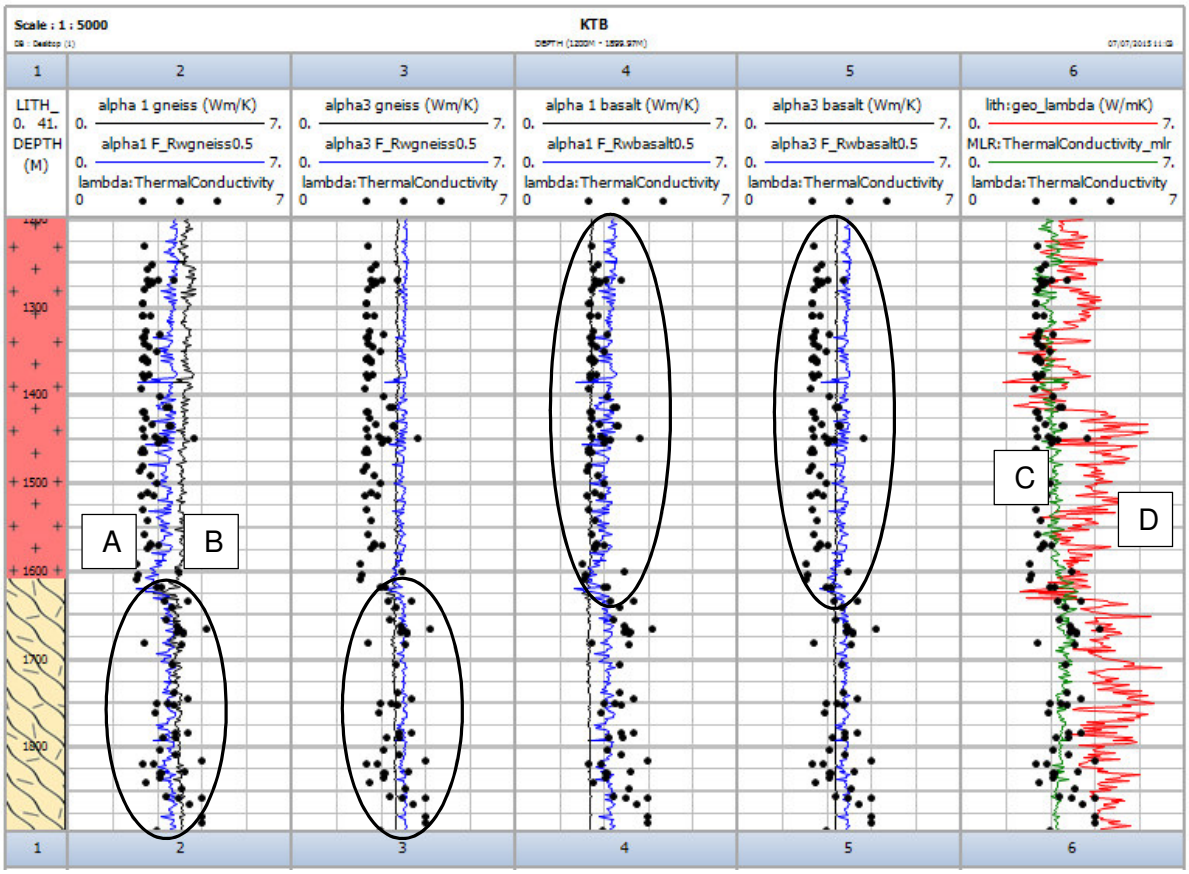

Figure 43: Comparison of thermal conductivity models for the lithologies granite/gneiss and basalt (Well KTB 1200-1900 meter): trace 1: lithology (cream with lines= gneiss, red with crosses= metabasite); trace 2,3 (gneiss): blue (A)= Resistivity estimated, black (B)= Sonic estimated; trace 4,5 (basalt): blue (A)= Resistivity estimated, black (B)= Sonic estimated; trace 6: green (C)=Multi Linear Regression, red (D)= Geometric-mean model

To compare the models for the lithology granite/gneiss and basalt, data of the KTB area 1200m to 1900m is observed in Figure 43. The models A (Resistivity estimated model), B (Sonic estimated model) and C (Muliple Linear Regression) show very homogeneous curves with no big spikes. Model D on the opposite changes very rapidly and has many spikes. Curves A, B and C are pretty similar and indicate a thermal conductivity in the same range. Model B is influenced by the lithology, the pore space and the pore filling. Model A only considers the shape of the pores and their filling. As mentioned before, model A is a little bit too high for the lithology basalt, especially in the case of aspect ratio 3 (smallest one). Model B provides a good range for the thermal conductivity estimation, especially for the lithology basalt.

The Geometric-mean model needs exact values for the mineral composition of the formation. For the KTB, XRD data is available and therefore an exact estimation of the mineralogy is possible. For most wells just cuttings are available and an exact calculation is not possible with this models.

Model A, B and C give a very good fit with the core data and can be applied. Model D return too high values and varies over a broad range, therefore this model cannot be recommended.

For the KTB a high amount of thermal conductivity data is available from cores. This high amount of samples points out the effect of anisotropy of every mineral. Therefore the real data scatters in a large area and an exact thermal conductivity value is not possible to make.

7. Conclusion

In most drilling projects Sonic log, Resistivity log and Gamma log are available. To measure thermal conductivity in a borehole is difficult and therefore petrographic-coded models for an indirect estimation are calculated and tested on real data of the continental deep drilling project in Germany (KTB).

For the model calculation the classification of the different lithologies on the basis of their formation factor and cementation factor is important to consider the form of the pore space. The pore space influences the thermal conductivity and therefore three aspect ratios are estimated for each lithology. The inclusion model is a good basis for the correlation of formation factor respectively compressional wave velocity with the thermal conductivity. The calculated regressions for the model deliver in general a good fit with the laboratory data and the three different aspect ratios give an admissible estimation window.

In the next step the models for granite/gneiss and basalt are applied on the log data. The Sonic log provides the values for the compressional wave velocity and is the basis for the first model estimation. The compressional wave velocity shows a strong connection with the thermal conductivity and therefore the calculated data fits the real data excellent.

With the Resistivity log the formation factor can be calculated and the second model can be applied. This model is influenced mostly by the pore shape and their fillings. For the lithology granite/gneiss it works well, but in the case of basalt the estimation is too high.

The calculated models show:

- No depth influence
- Strong correlation with the real data
- Dependence on lithology and pores/fractures (aspect ratio)

To compare the results of the two models also a multiple linear regression is calculated. This regression delivers excellent results. Also the geometric-mean model is tested on the KTB data. Here the results don´t show a good correlation with the real data and the curve scatters too strong.

The results show that the models (excluded the geometric-mean model) can be applied on borehole data and give a good estimation of the thermal conductivity.

A challenging topic for the thermal conductivity estimation is the effect of anisotropy. Minerals show different values when measured along different axes and therefore the data spreads over a large area. For continuation of this applications also the lithologies phyllite, sandstone and mica schist have to be applied on borehole logs and therefore more wells would be needed.

8. Reference list

Archie, G.E., 1942. The Electrical Resistivity Log as an Aid in Determining Some Reservoir Characteristics. *Petroleum Technology*, pp.54–62.

Berryman, J., 1995. Mixture theories for rock properties. In *A Handbook of Physical Constants (American Geophysical Union, Ed.)*. pp. 205–228.

Bertani, R., 2012. Geothermal power generation in the world 2005-2010 update report. *Geothermics*, 41(2012), pp.1–29.

British Petroleum, 2013. Statistical review of the world energy 2013.

Bücker, C. & Rybach, L., 1996. A simple method to determine heat production from gamma-ray logs. *Marine and Petroleum Geology*, 13(4), pp.313–315.

Budiansky, B. & O'Connell, R.J., 1976. Elastic moduli of a cracked solid. *International Journal of Solids and Structures*, pp.81–97.

Fuchs, S., 2013. *Well - log based determination of rock thermal conductivity in the North German Basin*. Universität Potsdam.

Gasior, I. & Przelaskowska, A., 2014. Estimating thermal conductivity from core and well log data. *Acta Geophysica*.

Gegenhuber, N., 2013. Correlation of thermal conductivity and resistivity of carbonates from Austria. *Austrian Journal of Earth Sciences*, 106/2, pp.37–44.

Gegenhuber, N.M., 2011. *A petrographic-coded model- Derivation of relationships between thermal and other physical rock properties*. Montanuniversity Leoben.

Gegenhuber, N.M. & Schön, J.H., 2010. Anisotropy of thermal conductivity of a gneiss-experiments and models. In *EGU general assembly*. Vienna, pp. 23–26.

GeoForschungsZentrum Potsdam, 2015. The aims of the KTB project.

Hartmann, A., Rath, V. & Clauser, C., 2005. Thermal conductivity from core and well log data. *International Journal of Rock Mechanics and Mining Sciences*, 42, pp.1042–1055.

Lichtenecker, K., 1924. Der elektrische Leitunswiderstand künstlicher und natürlicher Aggregate. *Physikalische Zeitschrift 25 (8)*, pp.169–233.

Mavko, G., Mukerji, T. & Dvorkin, J., 2009. *The Rock Physics Handbook, Second Edition*, Cambridge University Press.

Schön, J.H., 2011. *Physical properties of rocks: A workbook*, Elsevier.

Sen, P.N., 1981. Relation of certain geometrical features to the dielectric anomalyof rocks. *Geophysics*, 46, pp.1714–1720.

Vosteen, H.-D. & Schellschmidt, R., 2003. Influence of temperature on thermal conductivity, thermal capacity and thermal diffusivity for different types of rock. *Physics and Chemistry of the Earth, Parts A/B/C*, pp.499–509.

Figure captions

Figure 1: Geographic position KTB-Germany (GEODIS Brno, 2008) 3
Figure 2: 4-point-light instrument 5
Figure 3: Ultrasonic measurement tool 7
Figure 4: Formation factor vs. effective porosity (points= experimental data, lines= calculated data from F1 (m=1) to F11 (m=2)) 9
Figure 5: Bulk modulus determination (granite/gneiss)(experimental data with linear regression) 10
Figure 6: Shear modulus determination (granite/gneiss)(experimental data with linear regression) 10
Figure 7: Thermal conductivity vs. effective porosity (points=experimental data sorted after cementation factor m, lines= calculated data with different aspect ratio α) 12
Figure 8: Thermal conductivity vs. formation factor (points=experimental data, lines=calculated data with different aspect ratios and cementation factors e.g. red line= low aspect ratio and low cementation factor) 13
Figure 9: Thermal conductivity vs. v_p (points=experimental data, lines= calculated data with different aspect rations) 13
Figure 10: Thermal conductivity vs. formation factor (phyllite) (points=experimental data, curves= calculated data with different aspect ratios and cementation factors e.g. orange line= low aspect ratio and low cementation factor) 16
Figure 11: Thermal conductivity vs. compressional wave velocity (phyllite) (points= experimental data, curves= calculated data for different aspect ratios) 17
Figure 12: Formation factor vs. effective porosity (mica schist) (points, triangles= experimental data, lines= calculated data from F1 (m=1) to F11 (m=2)) 18
Figure 13: Thermal conductivity vs. formation factor (mica schist) (points, triangles=experimental data, curves= calculated data with different aspect ratios and cementation factors e.g. orange line= low aspect ratio and low cementation factor) 18
Figure 14: Thermal conductivity vs. compressional wave velocity (mica schist) (points, triangles = experimental data, curves= calculated data for different aspect ratios) 19
Figure 15: Formation factor vs. effective porosity (sandstone) (points, triangles= experimental data, lines= calculated data from F1 (m=1) to F11 (m=2)) 20
Figure 16: Thermal conductivity vs. formation factor (sandstone) (points, triangles=experimental data, curves= calculated data with different aspect ratios and cementation factors e.g. orange line= low aspect ratio and low cementation factor) 21
Figure 17: Thermal conductivity vs. compressional wave velocity (sandstone) (points, triangles= experimental data, curves= calculated data for different aspect ratios) 21

Figure 18: Formation factor vs. effective porosity (basalt) (points, triangles= experimental data, lines= calculated data from F1 (m=1) to F11 (m=2)) 22
Figure 19: Thermal conductivity vs. formation factor (basalt 1) (points =experimental data, curves= calculated data with different aspect ratios and cementation factors e.g. orange line= low aspect ratio and low cementation factor) 23
Figure 20: Thermal conductivity vs. compressional wave velocity (basalt 1) (points= experimental data, curves= calculated data for different aspect ratios) 24
Figure 21: Flow Chart of working plan for model calculation 25
Figure 22: Well KTB (1100 to 1900 meter): trace 1: lithology (cream with lines= gneiss; red with crosses= metabasite); trace 2: corrected-gamma-log, self-potential-log, caliper log; trace 3: Vp calculated from Sonic log and density log; trace 4: lines= calculated thermal conductivity gneiss for different aspect ratios, points= core data; trace 5: lines= calculated thermal conductivity basalt for different aspect ratios, points= core data 26
Figure 23: Well KTB (2800 to 3900 meter): trace 1: lithology (cream with lines= gneiss; red with crosses= metabasite); trace 2: corrected-gamma-log, self-potential-log, caliper log; trace 3: vp calculated from Sonic log and density log; trace 4: lines= calculated thermal conductivity gneiss for different aspect ratios, points= core data; trace 5: lines= calculated thermal conductivity basalt for different aspect ratios, points= core data 27
Figure 24: Well KTB (1200 to 1900 meter): trace 1: lithology (cream with lines= gneiss; red with crosses= metabasite); trace 2: corrected-gamma-log, self-potential-log, caliper log; trace 3: Laterolog Deep; 4: calculated formation factor 5: lines= calculated thermal conductivity gneiss for different aspect ratios, points= core data; trace 6: lines= calculated thermal conductivity basalt for different aspect ratios, points= core data 29
Figure 25: Well KTB (1200 to 1900 meter): trace 1: lithology (cream with lines= gneiss; red with crosses= metabasite); trace 2: corrected-gamma-log, self-potential-log, caliper log; trace 3: red= Laterolog deep, green= Neutron Log; trace 4: lines= calculated thermal conductivity gneiss for different aspect ratios, points= core data; trace 5: lines= calculated thermal conductivity basalt for different aspect ratios, points= core data 30
Figure 26: Well KTB (2800 to 3900 meter): trace 1: lithology (cream with lines= gneiss; red with crosses= metabasite); trace 2: corrected-gamma-log, self-potential-log, caliper log; trace 3: red= Laterolog deep, green= Neutron Log; trace 4: lines= calculated thermal conductivity gneiss for different aspect ratios, points= core data; trace 5: lines= calculated thermal conductivity basalt for different aspect ratios, points= core data 31
Figure 27: Comparison real data with Sonic calculated thermal conductivity (granite/gneiss); y-axis= thermal conductivity real data; x-axis= thermal conductivity estimated from Sonic log; colors mark the depth zones 32

Figure 28: Comparison real data with resistivity calculated thermal conductivity (granite/gneiss); y-axis= thermal conductivity real data; x-axis= thermal conductivity estimated from Resistivity log; colors mark the depth zones 33
Figure 29: Comparison real data with Sonic calculated thermal conductivity (basalt); y-axis= thermal conductivity real data; x-axis= thermal conductivity estimated from Sonic log; colors mark the depth zones 34
Figure 30: Comparison real data with resistivity calculated thermal conductivity (basalt); y-axis= thermal conductivity real data; x-axis= thermal conductivity estimated from Resistivity log; colors mark the depth zones 35
Figure 31: Cross plots gneiss; y-axis= thermal conductivity estimated from Resistivity log; x-axis= thermal conductivity estimated from Sonic log (left side alpha 1, right side alpha 3); colors mark the depth zones 36
Figure 32: Cross plot basalt; y-axis= thermal conductivity estimated from Resistivity log; x-axis= thermal conductivity estimated from Sonic log (left side alpha 1, right side alpha 3); colors mark the depth zones 37
Figure 33: Measured thermal conductivity (Well KTB from 2800 to 3500 meter) (gneiss); x-axis= thermal conductivity (W/mK) 38
Figure 34: Sonic calculated thermal conductivity (Well KTB from 2800 to 3500 meter) (gneiss); x-axis= thermal conductivity (W/mK); blue= alpha 1, orange= alpha 3.....38
Figure 35: Resistivity calculated thermal conductivity (Well KTB from 2800 to 3500 meter) (gneiss); x-axis= thermal conductivity (W/mK); blue= alpha 1, orange= alpha 3 39
Figure 36: Measured thermal conductivity (Well KTB from 3600 to 3900 meter) (basalt); x-axis= thermal conductivity (W/mK) 39
Figure 37: Sonic calculated thermal conductivity (Well KTB from 3600 to 3900 meter) (basalt); x-axis= thermal conductivity (W/mK); blue= alpha 1, orange= alpha 3.....40
Figure 38: Resistivity calculated thermal conductivity (Well KTB from 3600 to 3900 meter) (basalt); x-axis= thermal conductivity (W/mK); blue= alpha 1, orange= alpha 3 40
Figure 39: Cross plot Muliple Linear Regression; Y-axis= thermal conductivity real data; X-axis= thermal conductivity calculated with Multiple Linear Regression; colors mark the depth zones 41
Figure 40: Multiple Linear Regression (Well KTB 3200-3900 meter): trace 1: lithology (cream with lines= gneiss; red with crosses= metabasite); trace 2: corrected-gamma-log, self-potential-log, caliper log; trace 3: line= calculated multiple linear regression, points= core data 42
Figure 41: Cross plot geometric-mean model; Y-axis= thermal conductivity real data; X-axis= thermal conductivity calculated with Geometric-mean model; colors mark the depth zones .43

Figure 42: Geometric-mean model (Well KTB 3200-3900 meter): trace 1: lithology (cream with lines= gneiss; red with crosses= metabasite); trace 2: corrected-gamma-log, self-potential-log, caliper log; trace 3: Neutron log; trace 4: line= geometric mean regression, points= core data 44
Figure 43: Comparison of thermal conductivity models for the lithologies granite/gneiss and basalt (Well KTB 1200-1900 meter): trace 1: lithology (cream with lines= gneiss, red with crosses= metabasite); trace 2,3 (gneiss): blue (A)= Resistivity estimated, black (B)= Sonic estimated; trace 4,5 (basalt): blue (A)= Resistivity estimated, black (B)= Sonic estimated; trace 6: green (C)=Multi Linear Regression, red (D)= Geometric-mean model 45

Table captions

Table 1: Aspect ratios and resulting depolarization factors 12
Table 2: Overview of the host properties and assumed aspect ratios for different lithologies14
Table 3: Regressions and coefficient of determination from calculated curves for different aspect ratios (granite/gneiss) (λ in W/mK, v_p in m/s).....16
Table 4: Regressions and coefficient of determination from calculated curves for different aspect ratios (phyllite) (λ in W/mK, v_p in m/s).....17
Table 5: Regressions and coefficient of determination from calculated curves for different aspect ratios (mica schist) (λ in W/mK, v_p in m/s) 19
Table 6: Regressions and coefficient of determination from calculated curves for different aspect ratios (sandstone) (λ in W/mK, v_p in m/s) 22
Table 7: Regressions and coefficient of determination from calculated curves for different aspect ratios (basalt 1) (λ in W/mK, v_p in m/s) 24
Table 8: Regressions and coefficient of determination from calculated modified formation factor curves for different aspect ratios (basalt and granite/gneiss) (λ in W/mK).....30
Table 9: Multiple Linear Regression Formular 42

Appendix A1

Mineral	λ [W/mK]	author
Quartz mean	6.50	Clauser, 2006
Biotite	2.02	Clauser and Huenges, 1995
White mica	2.28	Clauser and Huenges, 1995
Garnet- Almandine	3.31	Clauser and Huenges, 1995
Chlorite	5.15	Clauser and Huenges, 1995
Pyroxene-Enstatite	4.47	Clauser and Huenges, 1995
Plagioclase	2.31	Clauser and Huenges, 1995
Orthoclase	2.31	Clauser and Huenges, 1995
Amphibole	2.81	Clauser and Huenges, 1995

Appendix A2

Sample	Rock type	Lithology	λ	ρ_b	ρ_s	v_p dry	F	$\Phi_{eff.}$
			[W/mK]	[g/cm³]	[g/cm³]	[m/s]	[ ]	[ ]
P6/1	Granite/Gneiss (rich in biotite)	1	2.52	2.67	2.74	3559.7	232.6	0.126
S37/1/1	Gneiss (rich in biotite)	1	2.37			3691.9		0.34
S37/1/2	Gneiss (rich in biotite)	1	2.37	2.73	2.9	2357	143.81	0.353
OMV-T2/1	Flasergneiss	1	4.94	2.73	2.74	4944	325.94	0.94
OMV-T2/2	Flasergneiss	1	4.94	2.74	2.75	4936.9	563.4	0.6
OMV-T2/3	Flasergneiss	1	4.94	2.72		4995	376.8	0.63
OMV-T2/4	Flasergneiss	1	4.94	2.73		488.7	469.39	0.73
OMV-T1/1	Gneiss	1	3.63	2.65	2.72	532	254.98	0.267
OMV-T1/2	Gneiss	1	3.63	2.7	2.73	5941	223.59	0.126
OMV-T2/1	Gneiss	1	4.7	2.68	2.76		63.93	0.279
OMV-T2/2	Gneiss	1	4.7	2.74	2.78			0.234
OMV-T2/3	Gneiss	1	4.7	2.75			7.26	0.229
OMV-T3/1	Gneiss	1	1.69		2.78			0.494
OMV-T3/2	Gneiss	1	1.69	2.63	2.75	3472	72.45	0.443
GBA26	Gneiss	1	3.84	2.72				0.6
S5	Gneiss	1	3.3	2.58	2.7			0.285
S5/N	Gneiss	1	3.3	2.52	2.68			0.332
S6	Gneiss	1	4.36	2.63	2.72			0.211
S6/N	Gneiss	1	4.36	2.63	2.7			0.169
B54/1	Granite	1	2.9	2.67	2.68	3854.3	613.69	0.48
B54/2	Granite	1	2.9	2.69		3891.7	579.41	0.57
B54/3	Granite	1	2.9	2.64		4155.2	552.92	0.38
P1/1	Granite/Gneiss	1	2.69	2.64	2.71	2248.9	185.27	0.13
P1/2	Granite/Gneiss	1	2.69	2.67	2.72	2111.1	416.48	0.132
HML1/1	Granite/Gneiss	1	2.3	2.88	2.94		123.87	0.153
HML1/2	Granite/Gneiss	1	2.3	2.86	2.91		169.69	0.133
TM2/1	Granite/Gneiss	1	2.82	2.59	2.66		31.93	0.134
TM2/2	Granite/Gneiss	1	2.82	2.59	2.67		311.24	0.1
VE1	Granite/Gneiss	1	2.44	2.65	2.71	4255.4	233.57	0.126
VE2	Granite/Gneiss	1	2.44	2.65	2.71	4261.3	188.49	0.97
HMF1	Granite/Gneiss (fine grained)	1	2.92	2.71	2.78		124.59	0.144
HMF1N	Granite/Gneiss (fine grained)	1	2.92	2.71	2.77		127.21	0.144
HMF2	Granite/Gneiss (fine grained)	1	2.68	2.69	2.76		115.63	0.131
HMF2N	Granite/Gneiss (fine grained)	1	2.68	2.71	2.77		243.4	0.132
HMG1/1	Granite/Gneiss (coarse grained)	1	2.68	2.66	2.71		147.78	0.165
HMG2	Granite/Gneiss (coarse grained)	1	2.55	2.6	2.76		19.45	0.137
HMKS	Granite	1	2.85	2.62	2.71		72.17	0.163
P7/1	"Knollkopf"-gneiss	1	2.68	2.65	2.68	2916.9	232.4	0.118
P7/2	"Knollkopf"-gneiss	1	2.68	2.64	2.68	2928.8	29.29	0.15
S37/2	Migmatit Gneiss	1	5.9	2.6	2.67	497.8	312.29	0.52
TKB15/1/1	Migmatit Granite	1	2.74	2.64	2.7	455	349.19	0.112
TKB15/1/2	Migmatit Granite	1	2.74	2.67	2.7	4495.7	22.81	0.126
P13/1	Orthogneiss	1	3.16	2.61	2.65	242.9	381.89	0.117
P13/2	Orthogneiss	1	3.16	2.6	2.65		286.47	0.126
P11/1	Para(Bi-)gneiss	1	2.31	2.84	2.86	3846.7	565.77	0.87
P11/2	Para(Bi-)gneiss	1	2.31	2.86	2.87	4512.9	382.46	0.71
GA3/1	Gneiss	1	2.63	2.59	2.67		193.72	0.171
GA3/2	Gneiss	1	2.63	2.61	2.67		184.65	0.188
P2/1	Gneiss (rich in quartz)	1	3.45	2.95	2.95	3929.1	369.78	0.65
P2/2	Gneiss (rich in quartz)	1	3.45	2.92	2.94	4393.8	35.31	0.72

Sample	Rock type	Lithology	λ	ρ_b	ρ_s	v_p dry	F	$\Phi_{eff.}$
			[W/mK]	[g/cm³]	[g/cm³]	[m/s]	[ ]	[ ]
GA6/1	Gneiss (rich in pyrite)	1	2.31	2.65	2.73		185.23	0.133
GA6/2	Gneiss (rich in pyrite)	1	2.31	2.58	2.74		19.62	0.146
GA5/1	Gneiss	1	2.57	2.62	2.67	3442.7	239.89	0.137
GA5/2	Gneiss	1	2.57	2.62	2.68		185.61	0.18
TKB15/2/1	Granite	1	2.83	2.55	2.67	5186.9	357.48	0.83
TKB15/2/2	Granite	1	2.83	2.63	2.7	4392.4	189.63	0.93
TKB15/2/3	Granite	1	2.83	2.69	2.72	4647.3	52.98	0.82
B3/1	phyllite (rich in chlorite)	2	3.43	2.82	2.8	6477.1	124.27	0.63
B3/2	phyllite (rich in chlorite)	2	3.43	2.82		6138.9	127.99	0.52
B3/3	phyllite (rich in chlorite)	2	3.43	2.78		6276.7	133.94	0.63
B3/4	phyllite (rich in chlorite)	2	3.43	2.82		6232.7	124.48	0.52
B3/2/1	phyllite (rich in chlorite)	2	3.7	2.79	2.78	3986	313.26	0.84
B3/2/2	phyllite (rich in chlorite)	2	3.7	2.82		379.1	285.37	0.62
B3/2/3	phyllite (rich in chlorite)	2	3.7	2.8		4372.8	449.57	0.62
B3/2/4	phyllite (rich in chlorite)	2	3.7	2.79		454.2	369.77	0.64
B3/3/1	phyllite (rich in chlorite)	2	4.17	2.8	2.81	5566.7	172.26	0.52
B3/3/2	phyllite (rich in chlorite)	2	4.17	2.8		499.3	11.34	0.63
B3/3/3	phyllite (rich in chlorite)	2	4.17	2.83		549.3	326.14	0.43
B3/3/4	phyllite (rich in chlorite)	2	4.17	2.83		53.5	332.33	0.42
B31/1	phyllite (rich in chlorite)	2		2.82	2.8	4421.2	223.19	0.62
B31/2	phyllite (rich in chlorite)	2		2.72		4134.3	118.97	0.72
B31/3	phyllite (rich in chlorite)	2		2.82		4557.6	191.49	0.72
B32/1	phyllite (rich in chlorite)	2	3.19	2.77		5746	196.2	0.47
B32/2	phyllite (rich in chlorite)	2	3.19	2.76	2.76	5355	265.33	0.49
B32/3	phyllite (rich in chlorite)	2	3.19	2.76		5418.8	231.29	0.59
B32/4	phyllite (rich in chlorite)	2	3.19	2.76		533	177.95	0.49
B44/1	phyllite (rich in chlorite)	2	4.36	2.7	2.72	4866.5	183.9	0.75
B44/2	phyllite (rich in chlorite)	2	4.36	2.64	2.71	4965.2	197.2	0.66
B45	phyllite (rich in chlorite)	2	4.63	2.79	2.81		94.3	0.116
B61/1	phyllite (rich in chlorite)	2	2.73	2.74	2.74	5483.5	236.84	0.43
B61/2	phyllite (rich in chlorite)	2	2.73	2.75	2.74	5335.1	435.42	0.42
GQ4	phyllite (rich in chlorite, quartz)	2	4.52	2.65	2.72		295.8	0.132
B39/1	phyllite (rich in graphite)	2	3.6	2.83	2.81	32.9	344.75	0.78
B39/2	phyllite (rich in graphite)	2	3.6	2.72	2.73	4787	376.3	0.58
B39/2/1	phyllite (rich in graphite)	2	2.88	2.77	2.78	442	255.28	0.97
B39/2/2	phyllite (rich in graphite)	2	2.88	2.74	2.77	43.8	247.24	0.88
B4/1	phyllite (rich in graphite)	2	3.49	2.83	2.86	5575.9	17.25	0.88
B4/2	phyllite (rich in graphite)	2	3.49	2.82	2.84	5112.4	17.29	0.97
B4/3	phyllite (rich in graphite)	2	3.49	2.82	2.83	5128.6	2.96	0.17
B4/2/1	phyllite (rich in graphite)	2	3.34	2.83	2.86	566.4	12.28	0.126
B4/2/2	phyllite (rich in graphite)	2	3.34	2.8	2.83	5364.3	22.25	0.78
B41/1	phyllite (rich in graphite)	2	3.5	2.73	2.78	321.4	343.3	0.85
B41/2	phyllite (rich in graphite)	2	3.5	2.73	2.78	4586	17.44	0.131
B42/1	phyllite (rich in graphite)	2	3.55	2.82	2.87	426.1	151.1	0.9
B42/2	phyllite (rich in graphite)	2	3.55	2.76			193.11	0.89
B42/3	phyllite (rich in graphite)	2	3.55	2.83		4334.7	239.84	0.88
B42/2/1	phyllite (rich in graphite)	2	2.96	2.76	2.78	3437.3	227.19	0.98
B42/2/2	phyllite (rich in graphite)	2	2.96	2.69		451.5	33.22	0.79
B42/2/3	phyllite (rich in graphite)	2	2.96	2.79		468.6	22.5	0.78
N5/1	Phyllite	2	2.81	2.63	2.75	3956.6	85.27	0.197
TX1/1	Phyllite	2	3	2.63	2.71		281.5	0.143
TX1/2	Phyllite	2	3	2.64	2.71		212.2	0.168

Sample	Rock type	Lithology	λ	ρ_b	ρ_s	v_p dry	F	$\Phi_{eff.}$
			[W/mK]	[g/cm³]	[g/cm³]	[m/s]	[ ]	[ ]
B56/1	Phyllite	2	2.97	2.77			125.3	0.95
B56/2	Phyllite	2	2.97	2.81	2.83	5252.6	114.99	0.19
B56/3	Phyllite	2	2.97	2.77		4911.3	192.34	0.86
B57/1	Phyllite	2	2.53	2.72	2.78	4427	176.9	0.97
B57/2	Phyllite	2	2.53	2.71	2.85	5627.8	14.37	0.11
B58/1	Phyllite	2	3.7	2.7	2.73	453	186.3	0.8
B58/2	Phyllite	2	3.7	2.71		499.6	28.8	0.79
B58/3	Phyllite	2	3.7	2.71		4914.4	184.62	0.79
B58/4	Phyllite	2	3.7	2.71		4626.1	196.93	0.79
B58/2/1	Phyllite	2	2.8	2.74	2.76	459.9	134.16	0.79
B58/2/2	Phyllite	2	2.8	2.7		4525.5	133.21	0.1
B7	Phyllite	2	3.52	2.68	2.87		158.65	0.17
B71/1	Phyllite	2	3.88	2.79	2.79	66.1	189.33	0.73
B71/2	Phyllite	2	3.88	2.78		5115.4	191.82	0.12
B71/3	Phyllite	2	3.88	2.76		5931.1	21.53	0.13
B72/1	Phyllite	2	3.36	2.82	2.81	5163.2	187.1	0.113
B72/2	Phyllite	2	3.36	2.8		4972.6	191.24	0.92
B72/3	Phyllite	2	3.36	2.77		4758.3	232.64	0.71
B72/4	Phyllite	2	3.36	2.84			158.44	0.92
S38N	black phyllite/Quarzite	2		2.63	2.66	4338.8	147.73	0.58
S38/2	black phyllite/Quarzite	2		2.7	2.73		96.45	0.94
S38/2/1	black phyllite/Quarzite	2		2.69	2.72		133.64	0.77
S69/1	green phyllite (rich in anhydrite)	2	5.42	2.75	3.3	2673	43.83	
P8/1	Mica schist (rich in biotite)	3	2.72	2.74	2.75	3171.7	584.12	0.47
P8/2	Mica schist (rich in biotite)	3	2.72	2.74	2.75	4135.8	511.14	0.58
B59/1	Mica schist (rich in chlorite)	3	3.28	2.76	2.76	5222	557.18	0.52
B59/2	Mica schist (rich in chlorite)	3	3.28	2.75	2.76	5275.1	56.69	0.74
B59/3	Mica schist (rich in chlorite)	3	3.28	2.74	2.77	573.2	422.61	0.62
P5/1	Mica schist	3	3.66	2.59	2.72		111.99	0.24
S3	Mica schist	3	3.54	2.71	2.81			0.133
B18/1	Mica schist	3	3.38	2.92	2.93	498.9	41.72	0.52
B18/2	Mica schist	3	3.38	2.93	2.93	5165.8	282.9	0.51
B18/3	Mica schist	3	3.38	2.92	2.9	535.4	381.51	0.41
B18/4	Mica schist	3	3.38	2.95	2.92	5385.9	535.26	0.62
B2/1	Mica schist	3	2.94	2.74	2.76	4975.2	239.91	0.51
B2/2	Mica schist	3	2.94	2.75	2.75	493.7	267.4	0.51
B2/3	Mica schist	3	2.94	2.75	2.75	481.7	262.46	0.51
B2/4	Mica schist	3	2.94	2.76	2.74	492.4	282.96	0.52
B35/1	Mica schist	3	5.46	2.86	2.83	3995.9	276.6	0.74
B35/2	Mica schist	3	5.46	2.76	2.82	649.1	168.7	0.96
B36/1	Mica schist	3	4.54	2.68	2.68	4588.8	267.39	0.62
B36/2	Mica schist	3	4.54	2.69	2.68	4694.8	362.56	0.51
B36/3	Mica schist	3	4.54	2.66	2.68	4775.6	281.46	0.53
B36/2/1	Mica schist	3	5.98	2.7	2.69	4199.6	314.5	0.59
B36/2/2	Mica schist	3	5.98	2.67	2.69	4149.2	294.88	0.68
B36/2/3	Mica schist	3	5.98	2.65	2.69	4196.9	53.85	0.57
B36/2/4	Mica schist	3	5.98	2.71	2.69	436.1	335.35	0.58
B37/1	Mica schist	3	4.45	2.73	2.74	5775.7	38.43	0.38
B37/2	Mica schist	3	4.45	2.76	2.75	5248.8	457.6	0.48
B37/3	Mica schist	3	4.45	2.73	2.73	5668.4	323.81	0.39
B37/4	Mica schist	3	4.45	2.75	2.74	577	347.89	0.39
B37/2/1	Mica schist	3	4.45	2.68	2.69	566.2	427.64	0.28

Sample	Rock type	Lithology	λ	ρ_b	ρ_s	v_p dry	F	$\Phi_{eff.}$
			[W/mK]	[g/cm³]	[g/cm³]	[m/s]	[ ]	[ ]
B37/2/2	Mica schist	3	4.45	2.72	2.7	5111.1	464.14	0.39
B37/2/3	Mica schist	3	4.45	2.68	2.7	65.6	816.42	0.39
B37/2/4	Mica schist	3	4.45	2.73	2.7	5628.3	53.32	0.39
B38/1	Mica schist	3	3.29	2.74	2.78	4995.3	278.85	0.39
B38/2	Mica schist	3	3.29	2.77	2.77	4245	447.93	0.78
B17/1	Mica schist	3	2.49	2.83	2.84	5636.4	278.23	0.72
B17/2	Mica schist	3	2.49	2.81	2.82	535.3	286.22	0.51
B17/3	Mica schist	3	2.49	2.83	2.82	5576.3	36.63	0.61
B17/4	Mica schist	3	2.49	2.82	2.81	5111.4	314.88	0.62
B19/1	Mica schist	3	3.63	2.63	2.77	4188.5	188.57	0.111
B19/3	Mica schist	3	3.63	2.75	2.79	3292.4	165.8	0.134
B6/1	Mica schist (rich in chlorite)	3	2.79	2.76	2.75	4898.5	212.9	0.42
B6/2	Mica schist (rich in chlorite)	3	2.79	2.76	2.75	4922.1	321.16	0.42
B6/3	Mica schist (rich in chlorite)	3	2.79	2.77	2.74	4792.7	267.46	0.42
B6/2/1	Mica schist (rich in chlorite)	3	2.86	2.74	2.77	4392.4	242.6	0.6
B6/2/2	Mica schist (rich in chlorite)	3	2.86	2.71	2.73	3851.1	224.18	0.8
B6/2/3	Mica schist (rich in chlorite)	3	2.86	2.71	2.73	4382.2	227.72	0.59
OMV-T6/1	Mica schist (rich in garnet)	3	3.9	2.99	3	666.4	64.18	0.29
OMV-T6/2	Mica schist (rich in garnet)	3	3.9	2.99	3	6533.7	725.86	0.27
OMV-T6/3	Mica schist (rich in garnet)	3	3.9	2.88		5669	547.86	0.35
OMV-T15/1	Mica schist (rich in garnet)	3	4.7	2.76	2.76	598.8	356.8	0.36
OMV-T15/2	Mica schist (rich in garnet)	3	4.7	2.73	2.74	5892.9	867.23	0.46
OMV-T15/3	Mica schist (rich in garnet)	3	4.7	2.79		5946.6	634.71	0.27
TE4/1	Mica schist (rich in garnet)	3	4.79	2.77	2.8		613.41	0.45
TE4/2	Mica schist (rich in garnet)	3	4.79		2.83			0.47
KSGS1/1	Green schist	3		2.75	2.83	482.8	166.35	0.86
KSGS1/2	Green schist	3		2.76	2.81	5436.2	171.31	0.17
KSGS2/1	Green schist	3		2.75	2.81	5353.9	157.14	0.98
KSGS2/2	Green schist	3		2.72	2.81	579.1	144.43	0.116
B74/3	Mica schist (rich in quartz)	3	4.22	2.62		4474.8	36.46	0.86
B67/1	Mica schist (rich in quartz)	3	3.13	2.7	2.73	5218.7	219.56	0.74
B67/2	Mica schist (rich in quartz)	3	3.13	2.72		4987.4	239.95	0.74
B67/3	Mica schist (rich in quartz)	3	3.13	2.67		431.7	117.59	0.159
B67/2/1	Mica schist (rich in quartz)	3	3.53	2.69	2.72	416.9	182.75	0.16
B67/2/2	Mica schist (rich in quartz)	3	3.53	2.72		4652.8	231.41	0.77
B67/2/3	Mica schist (rich in quartz)	3	3.53	2.69		447.8	235.13	0.68
B67/2/4	Mica schist (rich in quartz)	3	3.53	2.69		4597	179.92	0.116
B1/1	Mica schist (rich in Ca)	3	2.3	2.76	2.75	491.5	12.79	0.63
B1/2	Mica schist (rich in Ca)	3	2.3	2.72	2.75	4972.6	111.4	0.127
B1/3	Mica schist (rich in Ca)	3	2.3	2.76	2.74	5148.4	125.95	0.64
P1/2	Mica schist	3	3.33	2.71	2.73		283.4	0.95
P4/1	Mica schist	3.1	3.45	2.72	2.76	2941.9	334.74	0.161
P4/2	Mica schist	3.1	3.45	2.73	2.79	213	36.18	0.28
B73/1	Mica schist (rich in quartz)	3.1	4.65	2.6	2.66	3554	337.12	0.187
B73/2	Mica schist (rich in quartz)	3.1	4.65	2.58		3449.8	248.32	0.168
B73/3	Mica schist (rich in quartz)	3.1	4.65	2.51		3755.5	452.41	0.144
B75/1	Mica schist (rich in quartz)	3.1	3.83	2.59	2.66	4529.5	252.87	0.27
B75/2	Mica schist (rich in quartz)	3.1	3.83	9.57		4615	257.6	0.14
B75/3	Mica schist (rich in quartz)	3.1	3.83	2.6	2.66	4714.6	252.64	0.145
OMV-T11/1	Mica schist	3.1	2.85	2.71	2.81	3811	162.73	0.398
OMV-T11/2	Mica schist	3.1	2.85	2.75	2.88	3727.1	127.36	0.438
OMV-T11/3	Mica schist	3.1	2.85	2.7		393.5	221.98	0.252

Sample	Rock type	Lithology	λ	ρ_b	ρ_s	v_p dry	F	$\Phi_{eff.}$
			[W/mK]	[g/cm³]	[g/cm³]	[m/s]	[ ]	[ ]
OMV-T11/4	Mica schist	3.1	2.85	2.71		379.3	82.87	0.477
P1/1	Mica schist	3.1	3.33	2.73	2.73		423.73	0.152
GBA38	Conglomerate	4	3.61	2.65	2.73	5452.8	165.75	0.84
GBA25	claystone	4	4.44	2.66	2.79		73.37	0.158
R11	Breccia	4	3.5		2.73			0.371
R12	Breccia	4	3.76			411.7		
TE5/1	Breccia	4	3	2.7	2.74	3786	215.21	0.11
TE5/2	Breccia	4	3	2.7	2.77	2817.7	132.95	0.151
B25/1	Metaarenite	4	3.58	2.73	2.75	552.6	312.12	0.3
B25/2	Metaarenite	4	3.58	2.76	2.75	5533.7	287.34	0.29
B25/3	Metaarenite	4	3.58	2.76	2.75	5421.3	245.53	0.39
B25/2/1	Metaarenite	4	3.64	2.76	2.75	5216.7	239.72	0.39
B25/2/2	Metaarenite	4	3.64	2.75	2.75	5263.7	234.86	0.49
B25/2/3	Metaarenite	4	3.64	2.75	2.75	5449.2	33.67	0.39
B25/2/4	Metaarenite	4	3.64	2.76	2.75	5346.7	228.36	0.49
B26/1	Metaarenite	4	3.43	2.76	2.76	518.2	286.72	0.84
B26/2	Metaarenite	4	3.43	2.77	2.73	4748.8	239.28	0.53
B26/3	Metaarenite	4	3.43	2.77	2.76	589.3	191.92	0.73
B27/1	Metaarenite	4	3.38	2.74	2.72	578.9	244	0.49
B27/2	Metaarenite	4	3.38	2.75		533.2	234.84	0.49
B27/3	Metaarenite	4	3.38	2.71		526.3	24.74	0.49
B27/4	Metaarenite	4	3.38	2.73	2.73	4912.4	231.11	0.69
B27/2/1	Metaarenite	4	4.3	2.78		68.5	61.56	0.19
B27/2/2	Metaarenite	4	4.3	2.76		5531.3	139.6	0.69
B27/2/3	Metaarenite	4	4.3	2.75		5725.8	13.96	0.99
B27/2/4	Metaarenite	4	4.3	2.77	2.76	588.7	87.86	0.98
B27/3/1	Metaarenite	4	4.74	2.73	2.73	4822.7	173.69	0.69
B27/3/2	Metaarenite	4	4.74	2.72	2.74	5178.7	132.96	0.79
B27/3/3	Metaarenite	4	4.74	2.69	2.74	5629.6	74.31	0.9
B27/3/4	Metaarenite	4	4.74	2.71	2.74		139.34	0.79
B28/1	Metaarenite	4	6.8	2.75	2.72	4635.5	324.8	0.53
B28/2	Metaarenite	4	6.8	2.74	2.72	4683.3	448.93	0.54
B28/3	Metaarenite	4	6.8	2.76		4863.9	353.85	0.53
B29/1	Metaarenite	4	3.51	2.78	2.73	4666.7	36.63	0.53
B29/2	Metaarenite	4	3.51	2.77	2.75	4815.5	335.81	0.53
B29/4	Metaarenite	4	3.51	2.78	2.73	4876.8	374.5	0.63
B29/2/1	Metaarenite	4	4.26	2.76	2.75	4938.1	37.13	0.42
B29/2/2	Metaarenite	4	4.26	2.75	2.75	545.7	391.93	0.63
B29/2/3	Metaarenite	4	4.26	2.77	2.75	4857.8	448.16	0.42
B29/2/4	Metaarenite	4	4.26	2.74	2.74	4923.6	3.64	0.53
B66/1	Metaarenite	4	3.24	2.72	2.72	517.7	333.84	0.53
B66/2	Metaarenite	4	3.24	2.66		491.2	375.6	0.53
B66/3	Metaarenite	4	3.24	2.7		4731.1	339.39	0.63
B66/4	Metaarenite	4	3.24	2.69		4729.9	31.4	0.64
B6/3	Metaconglomerate (fine grained)	4	2.35	2.68	2.7	3295.7	332.47	0.68
B6/4	Metaconglomerate (fine grained)	4	2.35	2.68	2.68		426.27	0.68
B6/2/1	Metaconglomerate (fine grained)	4	3.28	2.67	2.67	389.2	422.28	0.73
B6/2/2	Metaconglomerate (fine grained)	4	3.28	2.66	2.68	3569.6	49.12	0.73
B6/2/3	Metaconglomerate (fine grained)	4	3.28	2.66	2.68	3858.5	469.91	0.73
B6/2/4	Metaconglomerate (fine grained)	4	3.28	2.68	2.69	3636	386.61	0.63
B6/3/1	Metaconglomerate (fine grained)	4	3.8	2.64	2.67	428.9	237.69	0.74
B6/3/2	Metaconglomerate (fine grained)	4	3.8	2.66		4262	264.19	0.86

Sample	Rock type	Lithology	λ	ρ_b	ρ_s	v_p dry	F	$\Phi_{eff.}$
			[W/mK]	[g/cm³]	[g/cm³]	[m/s]	[ ]	[ ]
B6/3/3	Metaconglomerate (fine grained)	4	3.8	2.67		423	299.4	0.84
GBA37	Sandstone	4.1	2.18	2.36		1887.7	46.98	0.1141
OMV-T23/1	Quarzite	4.1	4.6	2.65	2.69	5464.5	261.9	0.186
OMV-T23/2	Quarzite	4.1	4.6	2.67	2.69	5484.5	265.99	0.178
OMV-T23/3	Quarzite	4.1	4.6	2.67		5484.5	259.4	0.151
OMV-T23/4	Quarzite	4.1	4.6	2.68		55	331.9	0.151
R13	Breccia	4.1	3.28	2.66	2.79	46.4	11.62	0.58
OMV4/1	Breccia	4.1		2.9	2.65		23.18	0.1661
OMV4/2	Breccia	4.1		2.7	2.64	1787.6	19.93	0.1686
TE7b/1	Conglomerate	4.1	3.28	2.53	2.72	324.3	88.38	0.428
TE7b/2	Conglomerate	4.1	3.28	2.47	2.71	2748.1	84.13	0.46
MWQS1/1/1	Conglomerate	4.1	3.43	2.68	2.74	536.9	291.9	0.231
MWQS1/1/2	Conglomerate	4.1	3.43	2.64	2.74		344.46	0.285
MWQS2/1/1	Conglomerate	4.1	2.52	2.44	2.74		179.7	0.863
MWQS2/1/2	Conglomerate	4.1	2.52	2.26	2.76	231.9	55.29	0.153
MWQS3/1	Conglomerate	4.1	3.3	2.38	2.72	3175.7	48.5	0.672
B29/3	Metaarenite	4.1	3.51	2.76	2.73	494.3	314.72	0.221
OMV-T4/1	Sandstone (with clay, marl)	4.1	2.27	2.53	2.66	2759.2	7.61	0.752
OMV-T4/2	Sandstone (with clay, marl)	4.1	2.27	2.5	2.67	321	78.94	0.688
OMV-T4/3	Sandstone (with clay, marl)	4.1	2.27	2.53		31	78.9	0.693
OMV-T5/1	Sandstone (with clay, marl)	4.1	2.1	2.5		4271	96.2	0.726
OMV-T5/2	Sandstone (with clay, marl)	4.1	2.1	2.5		4277.6	86.75	0.734
OMV-T5/3	Sandstone (with clay, marl)	4.1	2.1	2.45		4315.6	85.77	0.74
P3/1	Amphibolite	5	2.18	3.4	3.5	2686.7	328.54	0.99
P3/2	Amphibolite	5	2.18	3.6	3.6	2934	276.3	0.9
P9/1	Amphibolite	5	2.3	3.3	3.6	4928.6	488.1	0.68
P9/2	Amphibolite	5	2.3	3.5	3.6	5922.9	322.47	0.63
M1/1	Amphibolite (with scheelite)	5	2.85	2.8	2.89	3871.6	148.35	0.124
M1/2	Amphibolite (with scheelite)	5	3.12	2.62	2.71		177.4	0.138
M2/1/1/1	Amphibolite (with scheelite)	5	2.53	2.97	3.3	3389.6	17.66	0.114
M2/1/1/2	Amphibolite (with scheelite)	5	2.53	2.91	2.99		18.4	0.129
M2/1/2/1	Amphibolite (with scheelite)	5	2.43	2.95	3.4		195.96	0.139
M2/1/2/2	Amphibolite (with scheelite)	5	2.43	2.97	3.7		139.12	0.27
M3/1/1	Amphibolite (with scheelite)	5	2.41	2.92	3.1	3659.1	155.37	0.152
M3/1/2	Amphibolite (with scheelite)	5	2.41	2.97	3.6	3839.2	233.12	0.129
M3/2	Amphibolite (with scheelite)	5	2.96	2.67	2.74	3989.1	21.87	0.81
SB3	Amphibolite (with scheelite)	5	1.14	3.5	3.13		231.38	0.15
SB4/1	Amphibolite (with scheelite)	5	1.14	2.96	3		281.56	0.126
SB4/2	Amphibolite (with scheelite)	5	1.14	2.91	2.99		24.1	0.138
SB4/3	Amphibolite (with scheelite)	5	1.14	2.95	2.99		263.3	0.141
B1/1	Metabasalt	5	2.4	2.85	2.91	4614	13.21	0.125
B1/2	Metabasalt	5	2.4	2.84	2.91	4564.2	92.5	0.127
B1/3	Metabasalt	5	2.4	2.9	2.9	4571.1	18.5	0.125
B3/1	Metabasite	5	3.19	3.4	3.6	5173.6	151.82	0.73
B3/2	Metabasit	5	3.19	3.4	3.5	494.6	166.48	0.72
B3/3	Metabasit	5	3.19	3.5	3.6	5192.9	165.67	0.86
B4/1	Metabasit	5	2.68	2.92	2.95	5298.9	137.49	0.73
B4/2	Metabasit	5	2.68	2.92	2.93	5144.3	152.86	0.73
B4/3	Metabasit	5	2.68	2.94	2.99	563.5	147.17	0.83
B5/1	Metabasit	5	2.82	2.98	2.97	439	156.3	0.88
B5/2	Metabasit	5	2.82	2.97	2.96	4292.3	144.25	0.97
B5/3	Metabasit	5	2.82	2.99	2.99	434.8	157.77	0.97

Sample	Rock type	Lithology	λ	ρ_b	ρ_s	v_p dry	F	$\Phi_{eff.}$
			[W/mK]	[g/cm³]	[g/cm³]	[m/s]	[ ]	[ ]
B11/1	Metabasit	5	1.72	2.9	2.92	4568.8	91.96	0.147
B11/2	Metabasit	5	1.72	2.88	2.92	4473.1	94.83	0.147
B11/3	Metabasit	5	1.72	2.87	2.9	455.2	78.53	0.157
B22/1	Metabasit	5	3.8	2.96	3.2	2979.1	171.78	0.88
B22/2	Metabasit	5	3.8	2.98		359.9	27.4	0.88
B22/2/1	Metabasit	5	4.37	2.93	2.99	45.7	149.34	0.158
B22/2/2	Metabasit	5	4.37	2.87		4158.2	168.27	0.12
B22/2/3	Metabasit	5	4.37	2.94		5218.1	173.5	0.128
OMV-T33/1	Quartz andesite	5.1		2.28	2.65	3468.9	42.99	0.134
OMV-T33/2	Quartz andesite	5.1		2.3	2.65	3575.8	41.79	0.1253
OMV-T33/3	Quartz andesite	5.1		2.3		3685.6	54.17	0.1174
OMV-T14/1	Vulkanite	5.1		2.44		4534	184.23	0.889
OMV-T14/2	Vulkanite	5.1		2.42		4334.7	159.17	0.983
OMV-T14/3	Vulkanite	5.1		2.45		4464.3	171.68	0.828
OMV-T32/1	Vulkanite (rich in biotite)	5.1		2.46	2.65	4148.6	123.75	0.687
OMV-T32/2	Vulkanite (rich in biotite)	5.1		2.4	2.67		49.74	0.976
OMV-T32/3	Vulkanite (rich in biotite)	5.1		2.4		38.4	68.56	0.861

Lithology 1 = Granite/Gneiss
Lithology 2 = Phyllite
Lithology 3 = Mica schist 1
Lithology 3.1 = Mica schist 2
Lithology 4 = Sandstone 1
Lithology 4.1 = Sandstone 2
Lithology 5 = Basalt 1
Lithology 5.1 = Basalt 2